CONTROLLED SINGLET OXYGEN GENERATION VIA PLASMONIC HEATING OF GOLD NANORODS

A THESIS SUBMITTED TO

THE GRADUATE SCHOOL OF ENGINEERING AND SCIENCE

OF BILKENT UNIVERSITY

IN PARTIAL FULFILLMENT OF THE REQUIREMENTS FOR

THE DEGREE OF

MASTER OF SCIENCE

IN

CHEMISTRY

By

Tuğçe Karataş

August, 2015

CONTROLLED SINGLET OXYGEN GENERATION VIA PLASMONIC HEATING OF GOLD NANORODS

By Tuğçe Karataş

August, 2015

We certify that we have read this thesis and that in our opinion it is fully adequate, in scope and in quality, as a thesis for the degree of Master of Science.

_____

(Advisor) Prof. Dr. Engin Umut Akkaya

_____

Asst. Prof. Dr. Bilge Baytekin

_____

Asst. Prof. Dr. Fazlı Sözmen

Approved for the Graduate School of Engineering and Science:

_____

Prof. Dr. Levent Onural

Director of the Graduate School

ABSTRACT

CONTROLLED SINGLET OXYGEN GENERATION VIA PLASMONIC HEATING OF GOLD NANORODS

TUĞÇE KARATAŞ

M.S. in Chemistry

Supervisor: Prof. Dr. Engin Umut Akkaya

August 2015

Photodynamic therapy (PDT) is the up-and-coming and developing methodology in order to treat various cancer tissues. The success of therapeutic action is directly related to the presence of cytotoxic singlet oxygen (SO) in tumor tissues. However, the feasibility of PDT is bounded by two major factors, hypoxia and the requirement of incident light penetration through cancer tissue. With these considerations, we have combined aromatic endoperoxides and gold nanorods so as to accomplish the possible restrictions. In this project, we synthesized and characterized both PEGylated anthracenic endoperoxides and gold nanorods separately and then further characterization was achieved for the combination of gold nanorods and aromatic endoperoxides. We have successfully proved that the thermal decomposition of endoperoxide molecule was carried out by irradiation of gold nanorods that resulted in the generation of both singlet and molecular oxygen.

Keywords: Photodynamic therapy, gold nanorods, aromatic endoperoxides, singlet oxygen.

ÖZET

ALTIN NANOÇUBUKLARIN PLASMONİK ISITILMASI İLE SİNGLET OKSİJEN ÜRETİMİ

TUĞÇE KARATAŞ

Kimya Bölümü Yüksek Lisans Tezi

Tez Yöneticisi: Prof. Dr. Engin Umut Akkaya

Ağustos 2015

Fotodinamik terapi (FDT) son zamanlarda pek çok araştırmacı tarafından derinlemesine incelenen, gelecek vaat eden ve gelişmekte olan kanser tedavisi için uygulanan yeni bir tedavi şeklidir. Bu tedavi yöntemi ile kanserli hücrelerin yok edilebilmesi ortamda bulunan zararlı singlet oksijenin (SO) varlığıyla doğrudan ilişkilidir. Yapılan araştırmalar sonunda FDT'nin etkisini artırabilmenin iki önemli faktöre bağlı olduğu görülmüştür. Bunlardan biri hipoksiya, bir başka deyişle kanser dokularındaki moleküler oksijen yetersizliğidir. Oldukça önemli olan diğer problem ise kanserli hücreye uygulanan ışığın dokulardan ancak oldukça az bir kısmının geçebilmesidir. Bu iki sorunu göz önünde bulundurarak ve bu problemleri en aza indirebilmek için aromatik endoperoksitler ile fonksiyonlandırılmış altın nanoçubuklar kullanmayı hedefledik. Bu proje kapsamında suda çözünebilen endoperoksit molekülleri ve altın nanoparçacıklar sentezlendi ve her bir aşamada tüm ürünler karakterize edildi. Ve bu proje ile ışıkla uyarılan altın nanoparçacıkların ısınması ve yüzeylerinde bulunan endoperoksitlerin bozunarak zararlı singlet oxygen açığa çıkarması ile amaçlandığı üzere kanser hücrelerinin ölümü gerçekleşmiştir.

Anahtar Kelimeler: Fotodinamik terapi, altın nanoçubuklar, aromatik endoperoksitler, singlet oksijen.

Dedicated to my mother and father

ACKNOWLEDGEMENTS

I would like to present my sincere gratitude to my supervisor Prof. Engin U. Akkaya for his endless support, guidance, and patience. He is the most intelligent, foreseeing, and the funniest person in my life. Being a member of Prof. Akkaya's research group is the most right decision in my life. I will never forget his support throughout my life.

I would like to thank Dr. Safacan Kölemen for being a brother for me and for his endless support, patience, and guidance to everything present in this thesis. He presented all his experience to improve my skills and knowledge in that laboratory process. I feel myself very lucky to meet him and to work with him.

I owe a special thanks to Dr. Tuğba Özdemir Kütük, Cansu Kaya, Ceren Çamur, Darika Okeev, Hale Atılgan, Jose Luis Bila, Melek Baydar and Tuğçe Durgut for their close friendships, endless support, help and understanding. We share everything and help to each other whenever we need. I will miss being and working with them.

I am sincerely grateful to our past and present members Dr. Fazlı Sözmen, Dr. Murat Işık, Dr. Ruslan Guliyev, Dr. Sündüs Erbaş Çakmak, Dr. Esra Tanrıverdi, Dr. Onur Büyükçakır, Dr. Yusuf Çakmak, Nisa Yeşilgül, Işın Sakallıoğlu, Taha Bilal Uyar, Ahmet Atılgan, Yiğit Altay, Dr. Dilek Taşgın, Dr. Özlem Seven, Özge Yılmaz, Deniz Yıldız, Abdurrahman Türksoy, Dr. İlke Şimşek Turan, Dr. Tuna Subaşı and rest of the SCL (Supramolecular Chemistry Laboratory) members.

I would like to express special thanks to my mother Fatma Arzu Karataş and father Muammer Karataş for their endless love, support and understanding. I owe them a lot.

Finally, I would like to thank my love Sinan Altuğ Ataş for his great love, support, patience and understanding.

LIST OF ABBREVIATIONS

PDT	**:**	Photodynamic therapy
ROS	**:**	Reactive oxygen species
HPD	**:**	Haematoporphyrin derivative
PS	**:**	Photosensitizer
LEDs	**:**	Light-emitting diodes
ISC	**:**	Intersystem crossing
BPD	**:**	Benzoporphyrin derivative
LSPR	**:**	Localized surface plasmon resonance
GNR	**:**	Gold nanorod
CTAB	**:**	Cetyltrimethylammonium bromide
PEG	**:**	Poly (ethylene glycol)
DMSO	**:**	Dimethyl sulfoxide
DMF	**:**	Dimethylformamide
EPO	**:**	Endoperoxide
TMS	**:**	Tetramethylsilane
$CHCl_3$	**:**	Chloroform
MS	**:**	Mass Spectroscopy
TLC	**:**	Thin layer chromotography
DPBF	**:**	Diphenylisobenzofuran
TEM	**:**	Transmission electron microscopy

Contents

List of Figures

List of Tables

1. INTRODUCTION

1.1. Photodynamic Therapy

1.1.1. General Information

Photodynamic therapy (PDT) has been accepted as a new therapeutic action for a number of disorders, especially for several forms of cancer such as malignant (head and neck, brain, urological, gynecological, dermatological, gastrointestinal cancers) and non-malignant tumors (age related macular degeneration-AMD, psoriasis).[1, 2, 3] The therapeutic action is affiliated with the photochemical reaction, which culminates the generation of singlet oxygen. Cytotoxic singlet oxygen is produced by irradiation of loaded photosensitizer in a targeted cell that leads to an energy transfer to molecular oxygen on cancer cells.[4] Thus, the basis of PDT requires the existence of three non-toxic components; molecular oxygen, photosensitizer, and light which initiate the production of highly reactive cytotoxic singlet oxygen. Singlet oxygen, and other reactive oxygen species (ROS) lead to the cell death because of their significant amount of toxicity.[5] So that, the cell death in PDT can be occurred in two different ways, apoptosis and necrosis. Furthermore, PDT can be applied any cancer patient either before or after the use of radiotherapy, chemotherapy, ionizing radiation or surgery which have serious side-effects resulted in damaging the functions of healthy cells.[4, 6] PDT is a non-invasive treatment method and patients can be treated many times with this therapeutic action. PDT will be investigated deeply in the following sections.

1.1.2. History of Photodynamic Therapy

Light-dependent therapeutic models, which have been applied by many researchers, date back more than three thousand years.[7, 8] The first attempts of using light in PDT were carried out by ancient Egyptian, Chinese and Indian in order to cure some diseases, such as psoriasis, rickets, vitiligo and even psychosis.[2] In the 2nd century BC, light-dependent therapy was defined as *"heliotherapy"* by Herodotes and it was used for restoration of human health.[9] At the nineteenth century lots of studies related to modern light therapy has been accomplished by different researchers. In 1900, the relation between the light at certain wavelength and chemicals was investigated by Oscar Raab.[10, 11] One of his experiment was related to the toxic effects of acridine on paramecia and in that study he investigated light-dependent treatment method accidentally thanks to strong thunderstorm.[12, 13] Four years later Herman Von Tappeiner who was the director of the Pharmacological Institute of the Ludwig-Maximilians University and A. Jesionek represented a new term *"photodynamic action"* after they treated skin tumors by collaborating white light and eosin.[14, 15] In the same year, Niels Finsen was rewarded with a Nobel Prize thanks to his studies related to treatment of cutaneous tuberculosis with the ultraviolet light. Thus, Niels Finsen evolved *"phototherapy"* which can be expressed as treatment of diseases by using light.[16]

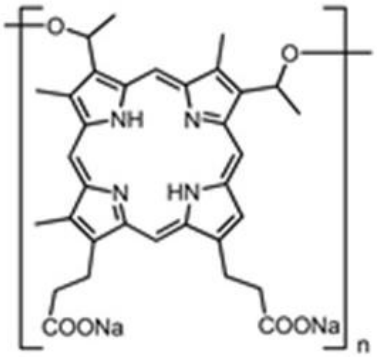

Photofrin (Hematoporphyrin Derivative)

Figure 1. The molecular structure of Photofrin

The most important photosensitizer to the enhancement of PDT is the haematoporphyrin that was firstly fabricated in an impure form by Scherer in 1841.[17] In the first 15 years of nineteenth century haematoporphyrin was used for many photobiological investigations, basically in order to demonstrate how it sensitized paramecia, mice[18], and humans[19] to light. Porphyrins can be described as a cyclic porphin based structure with a four pyrrole rings. These compounds was studied by W. Hausmann and his studies included haematoporphyrin and light in order to cure red blood cells and paramecium in 1911.[18] W. Hausmann's studies highlighted the first attempt to treat humans by using porphyrin derivatives. The German doctor Friedrich Meyer-Betz had very interesting experience after he injected haematoporphyrin to his own body. After the light interaction with this photosensitizer he reported swelling and pain.[19] PDT was accelerated by Richard Lipson and his collaborators at the Mayo Clinic in the 1960s.[20-23] They synthesized more improved haematoporphyrin derivative (HPD) which is called photofrin **1** (figure 1).[20] Besides Friedrich Meyer-Betz's experiences with haematoporphyrin, these former version of HPD could be injected in small amounts, because it can easily accumulate in tumor tissues. I.

Diamond and coworkers reported the first *in vivo* studies which demonstrated the retardation of brain-tumor growth in rats for almost 20 days.[24] In 1975 Thomas Dougherty and his colleagues represented so important improvement in PDT. Their studies involved injection of HPD and using red light which resulted in the extinction of tumor in mice.[25] After the remarkable improvements of animal experiments in PDT, first attempt with HPD for cancer patients was effectuated by Kelly and colleagues in 1976. They used HPD for both diagnosis and treatment of cancer tissue. According to their report the bladder cancer tissue could be diagnosed in five patients. Furthermore, this sensitizer was applied to cure one patient who experienced failures of radiotherapy and chemotherapy for recurrent bladder tumor. HPD succeeded to decelerate the growth of bladder cancer and it leaded to necrosis of the tissue.[26] Further studies performed by Dougherty *et al.*[27], O.J. Balchum and co-workers[28] and J.S. McCaughan *et al.*[29] demonstrated that PDT had promising results in different type of cancers such as breast[30], head and neck[31], pancreatic[32], gynaecological[33], brain tumors[34] if they were treated at their early-stages.

The most widely used photosensitizer, Photofrin (figure 1), was approved especially for the bladder cancer therapy first time in 1993.[1] As of the synthesizing partially purified derivative of HPD (Photofrin), it was applied for early-stage lung, gastric, cervical dysplasia, oesophageal tumors and also for advanced-stage lung and oesophageal cancers in many countries. Furthermore, there are many photosensitizers which got FDA approvals (Table 1) for photodynamic therapy can be denominated as m-THPC (Foscan) for head and neck tumors, 5-ALA benzylesther (Benzvix) for gastrointestinal tumor, 5-ALA hexylesther (Hexvix) for diagnosis of bladder tumors.[35]

Table 1. Clinically applied photosensitizers for malignant diseases[1, 36]

Photosensitizer	Structure	Activation Wavelength (nm)	Cancer Type
Porfimer sodium(HPD)	Photofrin	630	Cervical, lung, bile duct, gastric, bladder, brain tumours
Tin ethyletiopurpurin(SnET2)	Purlytin	660	Cutaneous, prostate, breast, basal-cell tumours
Boronated photoporphyrin	BOPP	630	Brain carcinoma
5-ALA	Levulan	635	Basal-cell, head and neck, gynaecological tumors
5-ALA methylesther	Metvix	635	Basal-cell tumors
5-ALA hexylesther	Hexvix	375-400	Diagnosis of bladder cancers
Taporfin sodium	Talaporfin	664	Solid tumors
Motexafin lutetium (Lutex)	Texaphyrin	732	Breast carcinoma
Padoporfin (TOOKAD)	Bacteriochlorin	762	Prostate cancers

1.1.3. Major components of Photodynamic Therapy

In order to understand the PDT action extensively, it is important to note that the principle of PDT involves three fundamental components: a photosensitizer, visible light and molecular oxygen ($^3O_2$). The efficiency of therapeutic action is directly related to the feature of photosensitizer (PS). Easy production process with low cost and good stability after manufacturing make PS an ideal agent for PDT. High absorption peak at longer wavelengths between 600-900 nm which is called therapeutic window is a critical interval for efficiency of PS. For example, 400 nm blue light can be used to illuminate superficial skin lesion, however it can only penetrate 1mm through lesion.[37, 38] Furthermore, the wavelengths of incident light longer than 900 nm do not have enough energy to generate cytotoxic singlet oxygen through energy transfer. Thus, it has been considered that penetration of incoming light through tissue is quite good at this therapeutic window.[39] PS should be individually non-toxic under dark condition that implies dark toxicity. Also, it should have minimum phototoxic side effect for healthy tissues. Another toxicity related property is having low systemic toxicity which defines longer retention time in tumor tissues and rapidly excretion from the body. The exquisite photochemical reactivity which directly affects the yield of singlet oxygen is another required property of a PS. Briefly, increasing the efficiency of PS during therapeutic action and decreasing its toxicity can be managed by functionalizing sensitizer.

The second requirement for PDT is light source. In this therapeutic action light is significant component both for inducing photochemical reaction and for the efficiency of PDT. Therapeutic window (600-900 nm) is the most effective interval for the

penetration of light through tissue as discussed before. Thus, as blue light could not penetrate easily through tissue, red light can penetrate more deeply.[39] Furthermore, longer wavelengths are not suitable to initiate the production of singlet oxygen because of their insufficient energy even if they can penetrate more deeply. There are lots of light sources for PDT depending on absorption spectrum of PS and the type of disease. The argon-pumped dye lasers and light-emitting diodes (LEDs) are most favored light sources for PDT. During the irradiation period in PDT its efficiency also depends on the total light dose, light delivery, and light exposure time.[36] The last significant component of PDT is molecular oxygen ($^3O_2$). It is necessary to generate cytotoxic singlet oxygen after irradiation of PS.

1.1.4. Mechanism of Photodynamic Therapy

In PDT action, the absorption of light by PS eventuates with the excitation of one electron from ground state of PS to a higher energy orbitals of singlet-excited state. At that point, this excited PS is very unstable and it will relax in two possible pathways. It can relax as emitting fluorescence so, it can turn back to ground state which is more stable. Alternatively, inter-system crossing (ISC) from singlet excited state to more stable triplet excited state is another most possible pathway if the photosensitizer involves transition metal complexes (Pt, Ru, Ir, Os)[40] or heavy atoms (iodine, bromine) or intramolecular spin convertors (C_{60}) without heavy atoms.[41] After ISC takes place and the excited PS transferred to the triplet state, there are also two possible reaction pathways for this excited triplet state sensitizer. Firstly, the activated PS can react with organic molecule in cell membrane so, PS transfer electron to molecule in order to

produce a radical. Then, unstable radicals will react with molecular oxygen ($^3O_2$) to form reactive singlet oxygen ($^1O_2$). In the second reaction, the excited PS can directly transfer its energy to molecular oxygen ($^3O_2$) that results in the formation of reactive $^1O_2$ (figure 2).[40, 42] One should note that each of reactions is molecular oxygen dependent so that *hypoxia* (the deficiency of oxygen) can prevent the efficiency of singlet oxygen in tumor tissues.

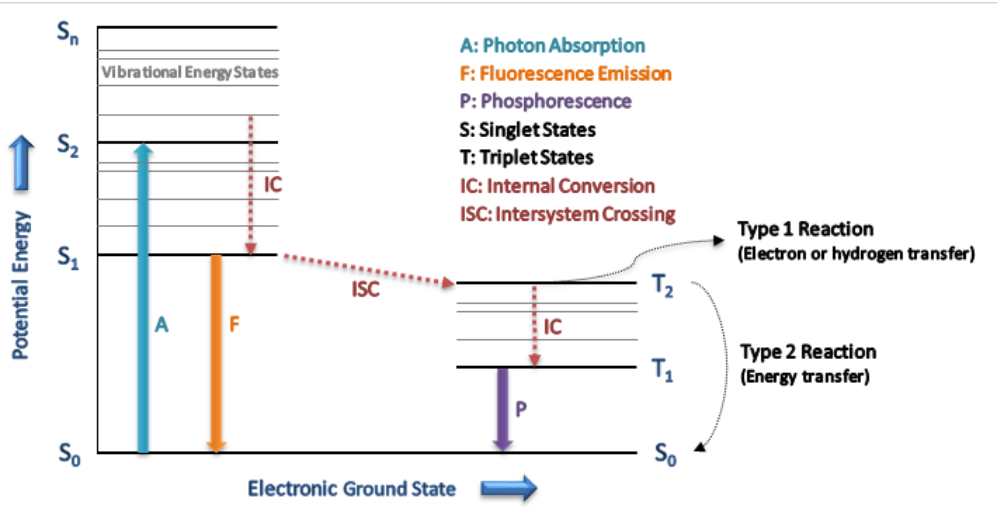

Figure 2. Modified Jablonski diagram for illustrating photosensitization processes

The highly reactive singlet oxygen has very short lifetime almost 10-320 ns and its diffusion in the aqueous medium is limited around 10 nm to 55 nm.[43] Photodamage with regard to the presence of reactive singlet oxygen can be carried out only if the cell and generated $^1O_2$ are close enough to each other. The photodynamic damage and cytotoxicity of PDT action are multifactorial and they are dependent on the type of sensitizer and its location, the injected dose of PS, the total dose of incoming light, and the presence of molecular oxygen in tumor tissue.[36] Thus, in order to increase the efficiency of PDT action all factor should be optimum coherency.

1.1.5. The effects of Photodynamic therapy on tumor tissues

In PDT action the product of photochemical reaction can activate tumor destruction in three possible ways. First one is the direct tumor death due to the presence of cytotoxic singlet oxygen. PDT action can also result in tumor destruction because of the damage in vascular system. The last case involves stimulation of immune system to damage tumor cell.[1] These all three results of PDT action serve for the tumor destruction and they provide long-term tumor control. The eradication of tumor cells can be occurred by direct photodamage after PDT action, but it is not the sufficient mechanism for the destruction of total tumor cells due to many reasons. One of the reason is that injected PS cannot distribute uniformly in cancer tissue.[44] Additionally, another possible reason, was reported by Mladen Korbelik and co-workers in 1995, is related to the insufficient tumor-cell killing because of the increase in the distance between vascular supply and cancer cells.[45, 46] The availability of molecular oxygen which can be directly used for the photochemical reaction during PDT action is the most possible limiting parameter for cancer cell eradication.[47] Thus, hypoxia and vascular damage after therapeutic action influence long-term tumor control negatively.

Further promising result of PDT for cancer treatment is damaging tumor vascular system. The existence and reproduction of tumor cells are directly dependent on blood vessels which carrying nutrients and oxygen. In 1989, vascular shutdown mechanism was performed with Photofrin-based PDT by Barbara Henderson and co-workers. They used a mouse with fibrosarcoma and therapeutic action triggered the damage in vascular system which decrease the oxygen supply to tumor cells.[48] One should note that the oxygen deficiency arising from vascular shutdown leads to decrease in tumor

growth. PDT based vascular damage and inhibition of tumor growth were experienced with other photosensitizers, Photofrin, HPD, and benzoporphyrin derivative (BPD). However, these studies reported that cycloxygenase and vascular endothelial growth factor were upregulated during PDT because of the generation of singlet oxygen and hypoxia resulted in PDT.[49]

The last parameter is the activation of immune system to strive against tumor cells. At the end of nineteenth century, the studies about the relation between PDT action and immune system showed that the penetration of lymphocytes, macrophages, and leukocytes through tissue was capable of activating the immune response for the destruction of tumor cells.[50, 51] Thus, immune system activated inflammatory process between healthy and cancerous cells will contribute damage of PDT-activated tumor tissue. For instance, in 1996 the retardation of tumor growth due to neutrophil accumulation, which can be determined as an immune response in PDT-treated tissue, was reported by Wil de Vree and co-workers.[52] The correlation between the immune system and PDT strengthen the effect of therapeutic action on tumor tissues so, PDT can be considered as a potential immune therapy.[1]

1.2. Gold Nanorods

The prime mover of nanotechnology, Richard P. Feynman, introduced his imaginary thoughts in his well-known talk, called as "*There's Plenty of Room at the Bottom*" in 1959. It is the first time to realize the possibilities of working with a nano-level by using atoms as a building blocks. In this manner, Feynman gave the opportunity to

many researchers to think and to develop the new, interesting, and fascinating area "nanotechnology". In the light of Feynman's thoughts, E. Dexter enhanced the idea of nanotechnology in his book which was entitled as "*Vehicles of creations: the arrival of the nanotechnology era"* in 1986.[53] Nanoscience, considering its birthdate which is around half century ago, is a highly promising field, and it is being used and developing in different business sectors like cosmetics, electronics, textile, medicine and many more. For the nanotechnological developments, nanoparticles have great attention due to their promising applications in optical devices, plasmon-enhanced spectroscopies, and biomedical technologies.[54] The chemical and physical properties of nano-scale matters are different than bulk system and these properties are mostly defined by the free electron motions.[55] In other words, the reduction of dimensions of bulk materials in 1-100nm scale affects its physical and chemical properties owing to the restriction of electron motions. Thus, it is obvious that the free electron motions of a matter are contingent upon its size and shape. For instance, the materials with 2-10 nm scale which has smaller dimension than their Bohr radius exhibit new properties due to quantum confinement and large surface area-to-volume ratio.[56] In the case of metal nanoparticle the surface effect become considerable when its size is smaller than the electron mean free path. In accordance with these explanations, noble metal nanoparticles including gold nanoparticles have these properties. For instance, Au nanoparticles, which have the large surface area-to-volume ratio resulted in higher number of surface sites with more dangling bonds, exhibit higher degree of chemical reactivity and bonding properties.[55] Furthermore, Au nanoparticles have several properties, such as nonlocal dielectric responses, confinement-induced shifts of energy levels, and enhanced optical transition probabilities owing to the electron confinement

in the material.[57] With regard to all of these remarkable features, gold nanoparticles have been investigated in many research groups deeply (figure 3).

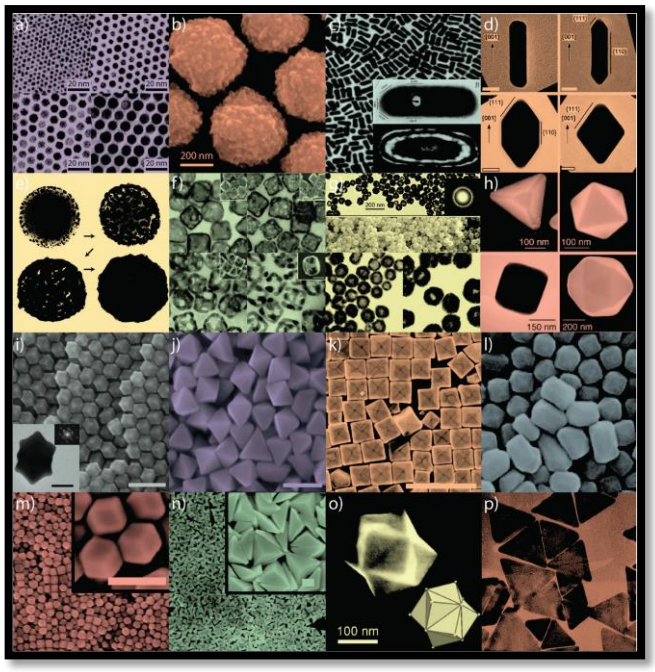

Figure 3. Gold nanoparticles with various size and shape. Copyright © 2011, Royal Society of Chemistry. Reprinted with permission from ref (62)[62]

Among all plasmonic nanoparticles, gold nanocrystals have a very important and remarkable property, localized surface plasmon resonance. In accordance with this property, Au nanoparticles can initiate the localized surface plasmon oscillations of the free electrons in a conduction band after the confinement of photons in their nanoscale size. Owing to the confinement of photons, Au nanoparticles have the ability to increase the amplitude of the light wave that provides the enhancement of electrical field.[58] Furthermore, localized surface plasmon resonance (LSPR) properties of Au nanoparticles can be accommodated in a desired range by tuning the shape and size of the particles in the course of chemical synthesis. Besides all other type of Au nanoparticles, gold nanorods (NRs) have an opportunity in the case of LSPR. Since, these rod-like shaped nanoparticles have two plasmon modes which are longitudinal

LSPR and transverse LSPR. Longitudinal one is comprised of the electron oscillations along the length axis, and transverse mode is induced by the light polarization along the transverse directions of Au nanorods. It is essential to note that; during chemical synthesis it is possible to tune the longitudinal LSPR wavelength of nanorods by changing the aspect ratios in order to cover the visible and near-IR regions.[56]

1.2.1. Plasmonic Properties of Gold Nanorods

The most exceptional and intriguing property of plasmonic nanoparticles is the localized surface plasmon resonances (LSPRs) that is the result of the confinement of conduction band electrons in a nano-scale as defined in a previous section. Owing to the resonant excitation, the ability to concentrate optical field in a region which is very close to the surfaces of nanoparticles enables the enhancement of electrical field, the scattering of light in higher degree, and the ability of plasmonic photothermal conversion.[54] Furthermore, the geometry of nanoparticle directly affects the plasmonic properties of the nanostructure. For instance, the plasmonic properties of symmetrical and dissymmetrical metal nanoparticles are quite different. Compared to their symmetrical counterparts, rod-like shape provides nanoparticles to strengthen their plasmonic behaviours.[54, 58] Regarding to the cylindrically symmetric gold nanorods, the conduction band electrons can move in two different directions that results in two distinct modes of gold NRs. In the transverse LSPRs of gold nanorods, the excitation of conduction electron oscillation along short axis exhibits a blue-shifted LSPR peaks around 500nm. However, in the longitudinal LSPRs of nanorods, the electrons move at the longer direction of gold NRs that result in the presence of longitudinal LSPR

peaks at red side of electromagnetic spectrum.[56] Furthermore, the energy of the longitudinal LSPRs of gold NRs is extremely affiliated with the aspect ratios.[59] So that by tailoring the ratio between the diameter and length of nanorods during chemical synthesis, it is possible to shift the maximum absorbance of longitunal LSPRs peaks from the middle of the visible region (~600 nm) to the near-IR region of electromagnetic spectrum (~1100 nm) (figure 4).[56] In addition to aspect ratio-dependence of longitudinal LSPR peaks the optical properties of gold NRs are strongly dependent on the dimensions of the particles.[59] In 2006, the dimension dependency of the scattering efficiency of gold NRs was investigated via calculations by Link and co-workers.[60] In pursuit of theoretical studies, the gold NRs with the same aspect ratio but different magnitude of dimensions were synthesized by Ali and collaborators in 2012. Their investigation showed that the larger gold NRs exhibited a greater extinction coefficient rather than gold NRs with small directions because of the scattering efficiency.[61, 62] It should be noted that the light scattering efficiency of larger gold NRs is quite better than smaller gold NRs. As a result of this feature, gold NRs with larger dimensions can perform better in optical imaging applications owing to its better scattering efficiency and smaller gold NRs can be applied in photothermal therapies owing to its better absorption efficiency.[59]

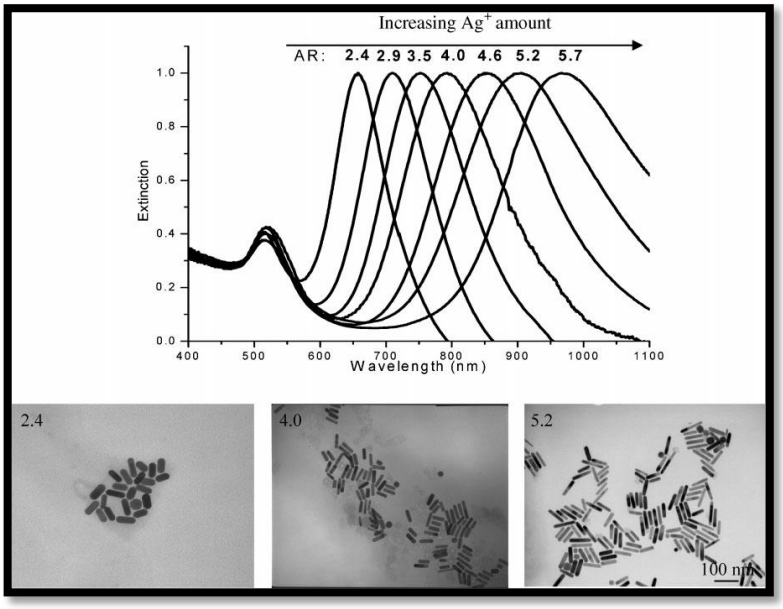

Figure 4. Plasmonic properties of gold nanorods with their different aspect ratios. Copyright © 2009 WILEY-VCH Verlag GmbH & Co. KGaA, Weinheim. Reprinted with permission from ref (56)[56]

The relaxation of absorbed energy through thermalization in gold nanoparticles will yield with the generation of heat which might lead to temperature increase on the surface of nanoparticles.[54] So that, this ability of generation of heat due to the plasmon resonance decay make gold nanoparticles to be excellent contributor for photothermal therapy, drug delivery systems and controllable drug/ gene release.[54, 56] By synthetically tailoring LSPR peaks of gold nanorods into the red region of electromagnetic spectrum, it can have strong light absorption and better tissue penetration in comparison with other light absorption species, such as spherical gold nanoparticles and organic dyes.[63] In this manner, gold nanorods have been investigated for photothermal conversion-based biomedical applications in recent years. For that applications the most important factor is the photothermal conversion efficiency of nanorods that involves the competition between radiative and non-radiative decays and the conversion efficiency is contingent upon the geometries and the plasmonic properties of gold nanorods.[54] The study of Chen and co-workers showed that gold

NRs will have highest photothermal conversion in case of better proximity between the wavelength of incident light and longitudinal LSPR wavelength of nanorods.[64] This condition provides the efficient excitation of gold NRs by incident laser. In addition to the dependency of plasmonic properties, geometry is another important factor for efficient photothermal conversion. According to theoretical and experimental investigations the volume of gold nanoparticles inversely affects the conversion efficiency. So that, effective photothermal conversion takes place in a small nanorods due to the reduced radiative decay that gives the ability of converting absorbed energy into heat. Furthermore, the concentration of applied gold NRs has additional influence on the photothermal conversion behaviors.[54] This concentration effects was investigated by Choi and collaborators and they showed that higher concentration of nanorods resulted in better photothermal conversion.[65, 66]

The determination of temperature distribution and heat formation on the surface of gold nanorods for photothermal conversion-based application, such as catalysis, hyperthermia, and microfluidics is very important. Until the study of Quidant and co-workers, only theoretical studies have been made and many efforts focused on spherical nanostructures.[54] In 2010 Quidant *et al.* presented a new technique to determine the local temperature on a single gold nanorod, thermal microscopy technique.[67, 68] Their method involves the determination of heat distribution on gold nanorod by using the molecular fluorescence polarization anisotropy and they showed that the local temperature of gold nanorod distributes uniformly in all directions.

1.2.2. Synthesis of Gold Nanorods

The first attempt for the synthesis of colloidal gold nanoparticles by reducing gold chloride in the existence of phosphorus was reported by Michael Faraday in 1857.[69] In the light of Faraday's study there have been many efforts in order to generate gold nanoparticles, involving nanoshells, nanorods, nanospheres, nanocubes, and other various type of nanoparticles. Thus, many methods that can be exemplified as photochemical reduction, electrochemical reduction, and chemical reduction have been achieved.[56, 70] Regarding to fabricating gold nanorods with high uniformity, quality, and yield two well-known procedures have been developed, top-down and bottom-up methods. The production of gold nanorods is obtained by combining lithography process with the deposition of gold crystals in top-down methods. However, in bottom-up method gold nanorod formation begins from the nucleation and growing of nanorods is achieved by the reduction of additional gold salts.[54]

The fabrication of gold nanorods by bottom-up methods involves some typical techniques, categorized as wet-chemical,[71] photochemical reduction,[72] electrochemical,[73] solvothermal,[74] and sonochemical techniques.[75] In these bottom-up methods, the growth of gold nanorods is carried out by reducing gold salts within some reducing agents, consisting of ascorbic acid and sodium borohydride. Furthermore, the elongation of gold nanorods along one direction during the reduction process is achieved by using templates. The first study related to templates was reported by Masuda and co-workers. In their study, anodic aluminium oxide membranes were used as a template in several bottom-up techniques.[76] Even if gold nanorods with high yield and uniform structure are obtained in the presence of aluminum oxide templates, many

efforts should be made in order to obtain pure nanorods without any residual of template.[54] So that, recent studies represented the more developed version of templates. The widely used template for the growth of gold NRs is cetyltrimethylammonium bromide (CTAB) which acts as a stabilizing agent and direct the longitudinal growth of gold nanorods.[77]

In literature, the most favored method for the fabrication of gold nanorods is the bottom-up, seed-mediated growth method was investigated by El-Sayed *et al* and Murphy *et al.* independently.[78, 79] Wet chemical seed-mediated growth method enables to obtain almost monodispersed, high yield and quality, and uniform gold nanorods.[54]

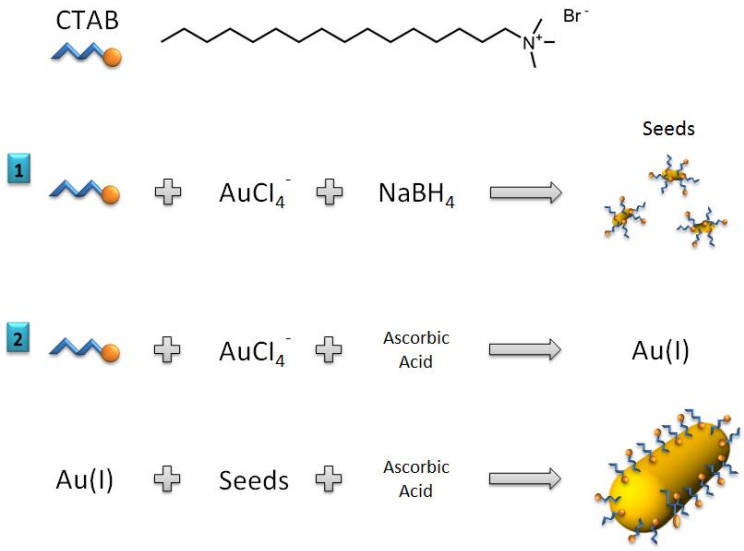

Figure 5. Mechanism of seed-mediated growth method for preparation of gold nanorods.

As it is represented in figure 5, seed solution which involves nearly 1.5 nm small gold nanoparticles are first synthesized by reducing chloroauric acid ($HAuCl_4$) by additional cold sodium borohydride ($NaBH_4$) in a CTAB solution. Afterwards, a little amount of seed solution is reacted with the growth solution which is prepared by

reducing $HAuCl_4$ supported by ascorbic acid in the existence of $AgNO_3$ in an aqueous CTAB solution. At that point, ascorbic acid provides the reduction of Au(III) to Au(I) and then, supplementary reduction of Au(I) to Au(0) is actuated by the addition of seed solution in order to fabricate gold nanorods. During the preparation of gold NRs the addition of $AgNO_3$ plays an important role to obtain high yield gold nanorods that refers to the proportion between the amount of rod-shaped nanoparticles to the total amount of nanostructures, including rods, spheres, shells, triangular plates in a solution.[77, 80] So that, the presence of $AgNO_3$ enables to control over the aspect ratio of nanorods.[81] In a detailed perspective, it is supposed that Ag^+ ions are attached to the {110} faces of gold nanoparticles; hence additional gold atoms will be accumulated on the {100} faces of nanocrystals that lead to the longitudinal growth of gold nanorods.[77] Consequently, seed-mediated growth method can produce nanorods with 99% yield. Furthermore, in this method it is possible to tailor the shape and size of gold nanorods while attentively arranging the growth conditions. The variable parameters for tuning size and shape of nanorods can be defined as the pH of the solution, temperature, the composition and concentration of surfactant, and the structure of the seed in the growth method.[82] In addition to the size and shape tuning of gold nanorods, the aspect ratios can be diverging between 2.4 and 8.5. For example, the aspect ratio of gold NRs is directly dependent on the concentration of $AgNO_3$, because Ag^+ ions are responsible for binding selectively to the high energy facets of nanorods. As well as many advantages of bottom-up method such as fabricating uniform and mono-dispersed nanorods with high yield, this method has also some drawbacks.[54] First possible problem is the unrestrained placement of gold nanorods during the growth method due to the random behavior of Au ions during the reduction

and deposition processes. Secondly, even if the same growth procedure is applied, the shape and size of gold nanorods can differ in each trial.

1.2.3. Functionalization of Gold Nanorods

The stability of gold nanorods under different conditions is achieved by functionalizing CTAB-coated gold nanorods with convenient inorganic and organic additives, also the functionalization provides to obtain intented reaction sites for other modifications.[58] Before introducing detailed informations regarding to functionalization of gold NRs through different methods, the influence of CTAB capping on the surface of Au nanorods should be emphasized. It is believed that the surface of nanorod is negatively charged as a result of the strong adsorption between gold surface and bromide ions. So that, the positively charged ammonium end of CTAB is capable of binding to bromide ions on the surface of gold nanorods by means of electrostatic interactions which yield with forming inner layer. The structure of CTAB molecule possesses two ends, ammonium head group and hydrophobic alkyl tails which does not like to be situated in water. Thus, another supplementary CTAB layer is formed, with hydrophobic carbon-chain end placing inside and ammonium head groups locating outside.[83] Ultimately, the existence of CTAB bilayer on gold nanorods provides the positive charge on the surface of rods and better stability in aqueous medium.[84] The interdigitated bilayer can be distorted as in the case of the lower CTAB concentration than the critical concentration for formation of micelle.

In general, for the functionalization of gold nanorods the affinity between gold and thiols is utilized. Small thiol-terminated molecules are not suitable due to the steric effect such that they are not capable to handle with the large attractive forces on rods. Thus, the reaction between small thiol molecules with gold NRs causes the aggregation of nanorods. Gold-thiol bonding chemistry mostly prefers thiol-terminated molecules with high molecular weights, such as poly(ethylene glycol)s (PEG)s to functionalize the gold NRs. Thiol-terminated molecules prefer to react with Au nanorods at the two ends that resulting in small packing density of CTAB at both ends.[85] Functionalization of gold NRs with thiol-terminated PEGs yields with PEGylated gold NRs with high stability and better biocompatibility, hence the retention time of these nanorods in aqueous medium is extended. Furthermore, PEGylated nanorods are capable of disperse in aqueous and several polar organic mediums, such as acetone, alcholos, acetonitrile, dimethyl sulfoxide (DMSO), dimethylformamide (DMF), and phosphate buffered saline solutions.[86] Surface modification of gold NRs can be obtained by disulfides and dithiocarbamates.[87] Besides Gold-thiol bond chemistry, there are some possible interactions, such as antibody-antigen interaction, electrostatic attraction, and DNA sequence recognition to modify the surface of gold nanorods.[54] For instance, the electrostatic attraction is observed in the deposition of negatively and positively charged polyelectrolytes on the positively charged surface of nanorods via a layer-by-layer deposition method.[88] Moreover, biological polyelectrolytes and proteins can be used to functionalize the surface of CTAB-coated nanorods by virtue of electrostatic adsorption. Also, further modification of gold nanorods can be accomplished with functional groups, like amine groups or carboxylic acid through the layer-by-layer technique.[54, 89]

1.2.4. Biological and Biomedical Applications of Gold Nanorods

One of the most important non-invasive therapeutic actions of metal nanoparticles is hyperthermia which depends on the photothermal conversion efficiency of nanocrystals. The irradiation of gold nanoparticles can be achieved by several items, such as ultrasound (acoustic waves), microwave irradiation, and near-infrared laser that allow local heating on cancer tissue.[90] Among all other metal nanocrystals, gold NRs are used commonly as a photothermal agent owing to high photothermal conversion ability, strong light absorption in near-infrared region, which causes the laser light penetration through deeper tissues, small size, and ease functionalizing for targeted cells.[54] Photothermal heating of nanorods results in the temperature increment on targeted site more than the normal body temperature (37°C), hence controlled increase in the local temperature has positive effects in cancer cells such that it triggers the tumor tissue death by disrupting the functionalities of DNA and RNA, denaturation of proteins, apoptosis/necrosis.[91, 92]

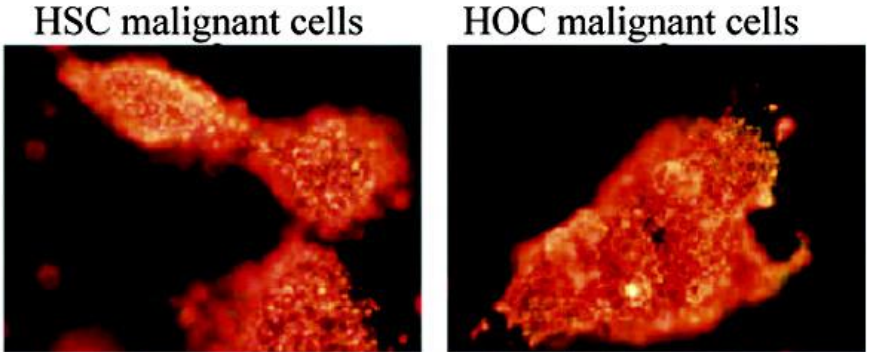

Figure 6. The photothermal therapy of malignant cells with anti-EGFR/Au by applying Ti: sapphire laser. Copyright © 2006, American Chemical Society. Reprinted with permission from ref (93)[93]

The first study for hyperthermic effect of gold nanorods was reported by El-Sayed and co-workers in 2006. The conjugated gold nanorods with anti-EGFR antibodies on

human oral tumor cells was irradiated with near-IR laser light(figure 6).[93] So that the study demonstrated that the theranostic effect of their designed nanorod resulted in both imaging of targeted region and hyperthermia on tumor tissue. The selective tumor region was firstly exposed by light scattering images of conjugated gold nanorods, and then it was irradiated by Ti: sapphire laser (red light at 800 nm).

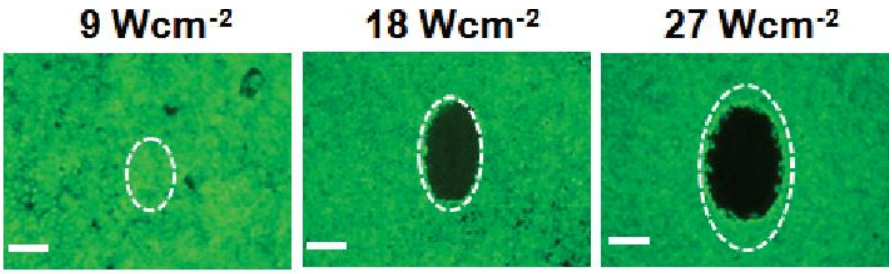

Figure 7. Photothermal therapy of A549 malignant cells with anti-EGFR/ Au by using NIR CW lasers. Copyright © 2010 WILEY-VCH Verlag GmbH & Co. KGaA, Weinheim. Reprinted with permission from ref (94).[94]

In 2009 Yeh and co-workers conducted experiment on photothermal effects of PEI/PSS- modified gold nanorods which were targeted on the death of A549 malignant cells. Figure 7 represented that the power of incident light is very important to damage the cancer cells. Since, it is obvious that even if 9 W cm^{-2} is not sufficient for cell death, 18 W cm^{-2} and 27 W cm^{-2} can damage the malignant cells.

The promising feature of the combination of photothermal therapy (PTT) and photodynamic therapy (PDT) was investigated by Choi and co-workers in 2011.[95] In their study PDT drug ($AlPcS_4$) and gold nanorods were combined to observe the dual therapeutic effect of PDT and PTT at the same cancerous region. So that, the complex of gold nanorod and photosensitizer can be used both to visualize and to treat various type of malignant tissues.

1.3. Polycyclic Aromatic Endoperoxides

1.3.1. General Information

The well-known property of polycyclic aromatic hydrocarbons is the ability of trapping reactive singlet oxygen in order to generate endoperoxide (EPO) molecules. In this manner, some of these generated endoperoxide molecules can release either singlet oxygen or triplet oxygen in their excited states in case of heating or irradiation of light.[96] In 1926 first studies related to endoperoxide compounds were carried out to investigate the dissociation process of rubrene. In the light of first investigation of endoperoxides, further studies included the dissociation behavior of 9,10-diphenylanthracene.[96] Among many other anthracenes, especially the endoperoxide form of 1,4-dimethoxy-9,10-diphenylanthracene can produce singlet oxygen at room temperature.[96] In 1964 Foote showed the further investigations regarding to singlet oxygen which was considered as an active species in photooxidation after irradiation of EPOs.[97] Foote's researches was improved by Rigaudy in order to demonstrate the relation between electron donating groups and dissociation temperature of EPOs. So that, Rigaudy showed that the dissociation temperature of 1,4-dimethyl- and 1,4-dimethoxy- naphthalene derivatives is lower than the EPOs of 9,10-diphenylanthracene.[98] Afterwards, many research groups have taken advantage of the reactive singlet oxygen in biological environments by sensitizing water-soluble endoperoxide of naphthalene derivatives.[99] In the light of several researches the substitution of polycyclic aromatic hydrocarbons in different position provides the control on dissociation of endoperoxides.

1.3.2. Preparation of Endoperoxides

In the literature there are almost 500 endoperoxide molecules which have been derived from polycyclic aromatic hydrocarbons and most of EPOs were generated by photosensitized oxygenation. This photosensitized oxygenation was described as a [4+2] cycloaddition of singlet oxygen to aromatic hydrocarbon.[100] Among all endoperoxide derivatives 3 fused benzenic compounds (anthracene) and higher members of acene compounds can easily undergo [4+2] cycloaddition reaction with $^1O_2$ whereas the aromatic molecules which has less than 3 fused benzenic core such as benzene and naphthalene cannot react with singlet oxygen.[96] Regarding to many studies it is obvious that the efficiency of reaction between singlet oxygen and the carbons of polycyclic aromatic compound depends on structural, steric factors and solvent effects.

The electron density of hydrocarbons directly enhances the efficiency of reaction between aromatic hydrocarbons and $^1O_2$ owing to the electrophilic nature of $^1O_2$. The number of fused ring of the aromatic hydrocarbons is one of the structural effects. In literature it is well known that EPOs can be synthesized from hydrocarbons which has fused benzenic cores range from 1 to 9. The studies with different ring number of acene series demonstrated that the reactivity of the substrate towards $^1O_2$ increases with the number of fused ring directly. For instance, Stevens and coworkers worked with different acene molecules such as anthracene, tetracene, and pentacene. Their studies showed that the number of fused ring increased the reactivity by about 2-fold.[101] Following factor which affects the reactivity of aromatic compound toward $^1O_2$ is related to the electron density on aromatic hydrocarbons. Aubry and coworkers

demonstrated the influence of electron donating groups on the reaction rate of $^1O_2$ addition. Regarding to their studies binding electron-releasing groups to the aromatic hydrocarbons, which will give the cycloaddition reaction with $^1O_2$, increases the reactivity of that hydrocarbons in the order $H < C_6H_5 < CH_3 \leq OCH_3$.[96]

Steric factor is another significant parameter which is able to affect both the reaction side of $^1O_2$ and the reactivity of aromatic hydrocarbon toward $^1O_2$. According to Erden and collaborators investigations [2,2] paracyclophane diene can be given as an example of steric effects on endoperoxide formation. Thus, this molecule, which has 2 benzene rings, is distorted in order to undergo the cycloaddition reaction of $^1O_2$.[102] Furthermore, peri interaction in 1,8-dimethylnaphthalene also plays an important role in the reactivity of aromatic compounds.[103] The presence of two methyl groups in that molecule relaxes the steric strain in the transition state in this manner peri interaction increases the reaction rate for endoperoxide formation. The last factor that affects the reaction rate of cycloaddition of $^1O_2$ is solvent effects. Regarding to many investigation with different solvent molecules, it is obvious that highly polar solvents increases the reaction rate more than other solvents. In 1995 Aubry and coworkers investigated the solvent dependency of rate constant of endoperoxide formation. They showed that the rate constant of $^1O_2$ cycloaddition to aromatic substrate increases from cyclohexane to water by more than 100-fold in case of water-soluble derivatives of aromatic compounds.[104]

In 2000 Bobrowski and collaborators performed the study of cycloaddition of singlet oxygen to benzene and this investigation revealed some differences between Diels-Alder reaction and [4+2] cycloaddtion of $^1O_2$ to aromatic hydrocarbon.[105] According

to their studies the suggested cycloaddition mechanism involves the single-step reaction between aromatic ring and singlet oxygen that is accomplished with the charge transfer from the organic donor to $^1O_2$.[96]

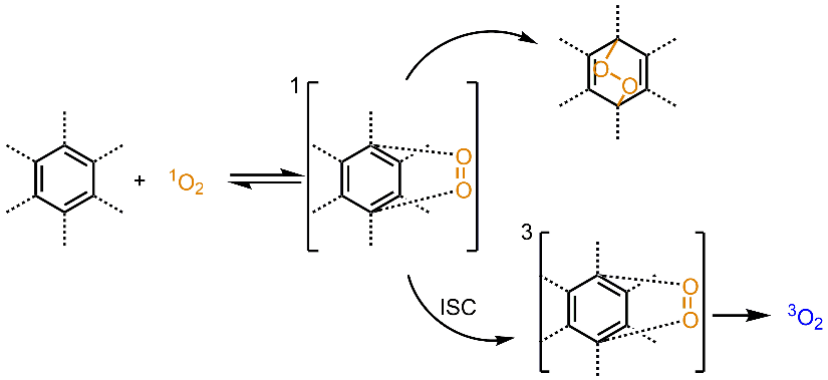

Figure 8. Mechanism of cycloaddition reaction of singlet oxygen.

The cycloaddition reaction involves mainly two steps (figure 8). In the first step reaction between aromatic ring and singlet oxygen will resulted in the reversible intermediate which is in the singlet state. Then, this intermediate can resulted in either the endoperoxide formation or dissociation into starting molecule and $^3O_2$. Molecular oxygen formation takes place because of spin-forbidden intersystem crossing (ISC).[106]

1.3.3. Thermal Dissociation of Endoperoxides

The thermal decomposition of endoperoxides results in two possible pathways; cycloreversion and homolytic cleavage. In a detailed explanation of two primary pathways: cycloreversion leads to starting compound and oxygen, in a triplet ($^3O_2$) or a singlet state ($^1O_2$), and homolytic cleavage of peroxide bond in EPO that leads to quinones and hydroxyl-ketones (figure 9).[107]

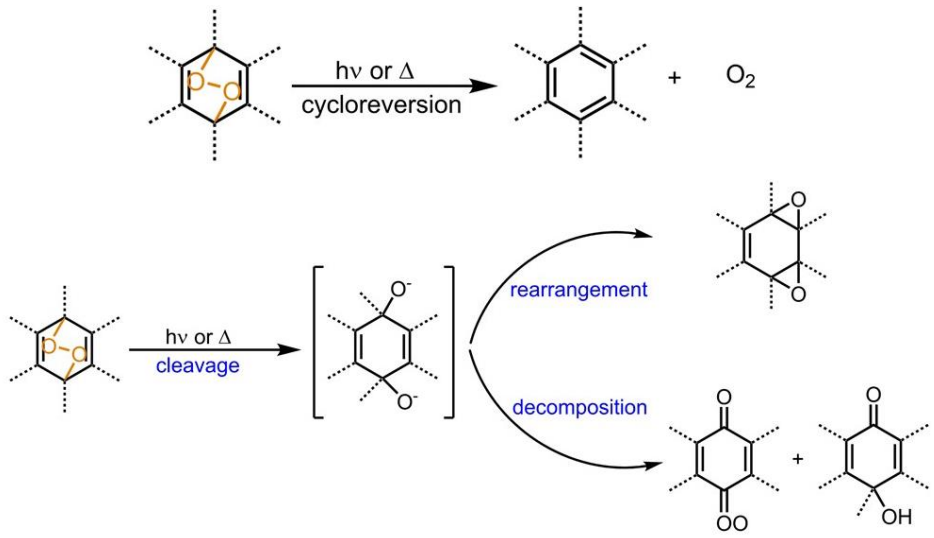

Figure 9. Thermal dissociation of aromatic endoperoxides.

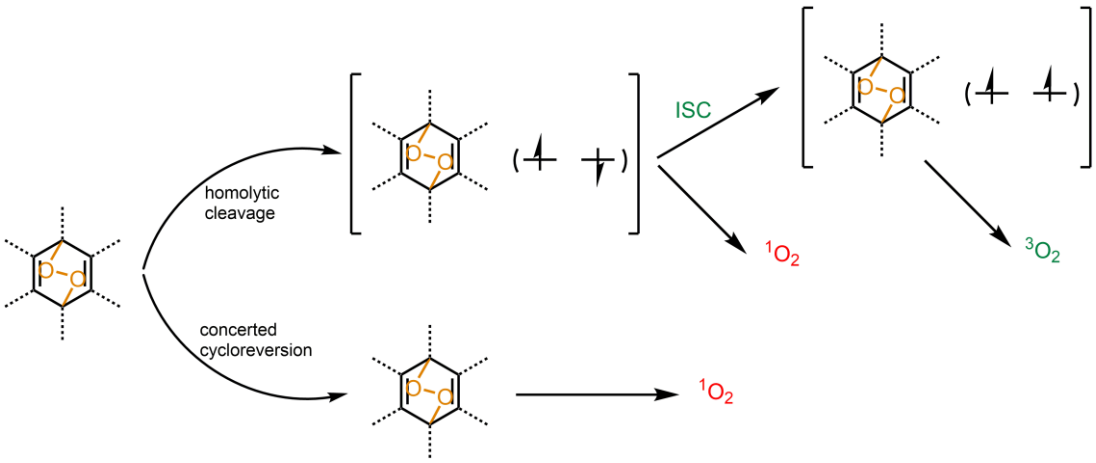

Figure 10. Thermolysis of cycloreversion pathway of aromatic endoperoxides.

After the thermal decomposition of EPOs, the competition between resulted pathways, cycloreversion and cleavage, is affected by the relative activation energies. The activation parameters for thermal decomposition of some endoperoxide molecules are listed in table 2.[96] So that regarding to that table, for cycloreversion pathways the magnitude of activation enthalpy of endoperoxide increases from unsubstituted benzene to naphthalene derivatives and to substituted anthracenic derivatives of endoperoxides. Furthermore, the higher values of activation enthalpies of anthracenic

derivatives leads to competition between cleavage and cycloreversion. However, the aromatic substitiution at bridgehead meso positions of endoperoxide provides the more favored cycloreversion process upon heating.[96]

In point of thermal cycloreversion process of endoperoxides, it also divides into two possible pathways. Cycloreversion can result in either homolytic cleavage, leading to oxygen molecules in singlet and triplet state due to ISC, or concerted cycloreversion mechanism which only produces singlet oxygen (figure 10). The singlet oxygen yield was investigated by Turro and coworkers and they found that 1,4- substituted naphthalenic and anthracenic EPO derivatives generated singlet oxygen in a high yield, however 9,10- type anthracenic EPOs decompose both singlet ($^1O_2$) and molecular oxygen ($^3O_2$) (table 2).[107]

Endoperoxide	$\Delta H^{\neq}$ (kJ/mol)	$\Delta S^{\neq}$ (J/K*mol)	$^1O_2$ (%)
	74.4±2	-1.7±8	90±3
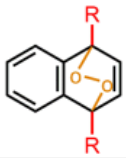	**a** 97.0±4 **b** 101.1±1	0.8±5 8.4±4	~100 76±1
	**c** 124.6±1 **d** 101.1±1	-7.5±3 -1.3±3	92±1 95±5
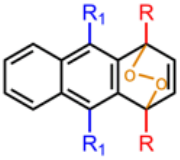	**e** 135.8±1 **f** 132.9±1	40.1±2 30.9±3	32±1 52±4

a: R = H. **b:** R = CH_3. **c:** R_1 = C_6H_5, R = CH_3. **d:** R_1 = C_6H_5, R = OCH_3. **e:** R_1 = C_6H_5, R = H. **f:** R = R_1 = C_6H_5.

Table 2. Activation parameters for thermal decomposition of several endoperoxide molecules.

2. EXPERIMENTAL PROCEDURE

2.1. General

In that project, all ^{1}H NMR and ^{13}C NMR spectra were recorded by using Bruker DPX-400, which is operating at 100 MHz for ^{13}C NMR and 400 MHz for ^{1}H NMR, in $CDCl_3$ or DMSO-d_6 with tetramethylsilane (TMS) as internal reference. All characterizations with NMR spectroscopy were performed at 25 °C. Coupling constants are presented as Hz and chemical shifts were recorded in parts per million (ppm). Absorption spectrometry was acted using a Varian Cary-100. Mass spectrometry measurements were performed with Agilent Technologies 6224 TOF LC/MS and 6530 Accurate Mass Q-TOF LC/MS. TEM images were obtained by using FEI Technai G2 F30 high-resolution transmission electron microscope and carbon grid. All reactions with regarding to aromatic endoperoxide derivative were monitored by thin layer chromatography using Merck TLC Silica gel 60 F_{254}. Silica gel column chromatography of all products was performed over Merck Silica gel 60 with particle size: 0.040-0.063 mm, 230-400 mesh ASTM.

2.2. Singlet Oxygen Trap Experiments

Singlet oxygen experiments were performed in organic solvent by using 1,3-Diphenylisobenzofuran (DPBF) as a singlet oxygen trap molecule. First of all, **(9)-GNR** conjugate and a trap molecule (DPBF) were mixed in DMSO, then several dark measurements were recorded in order to stabilize absorption peak of trap molecule.

Afterwards, **(9)-GNR** conjugate was irradiated at absorption maximum of GNR using laser light. Singlet oxygen generation was observed while monitoring absorbance decrease of trap molecule after the irradiation of the conjugate by incoming laser light. The instrument for irradiation of **(9)-GNR** conjugate was Tsunami, SpectraPhysics, USA laser system in combination with Spectrum Analyzer, SpectraSuite, Ocean Optics, USA. Excitation wavelength and power of light were adjusted to 830 nm and 1 W/ cm^2 respectively. **Laser irradiation was studied in Dr. Bulend Ortac research group at UNAM, Bilkent University, Ankara, Turkey.**

2.3. Synthesis of (2)

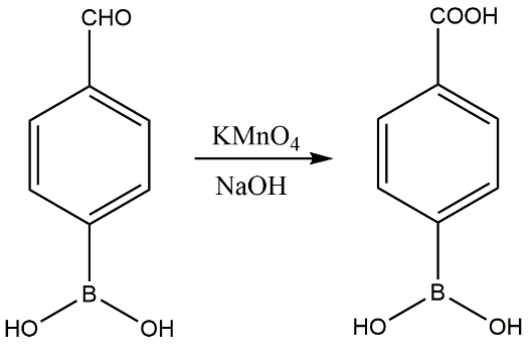

A commercial 4-formylboronic acid (1.0 g, 6.67 mmol) was dissolved in aqueous sodium hydroxide solution (5.4 mL of a 2.5 M solution). Then, the solution of 4-formylboronic acid was diluted with 40 mL distilled water. A freshly prepared solution of $KMnO_4$ (246 mg, 1.56 mmol, 0.23 eq.) in distilled water (7.5 mL) was added two times into the diluted 4-formylboronic acid solution at 1-hour intervals. The mixture was stirred overnight, after that ethanol (3 mL) was added and further stirring was maintained for 10 min at 50 °C. After cooling the reaction to room temperature, it was

filtrated over celite. The filtrate was acidified to pH 2.5 by the agency of 0.5 M HCl. After all procedure, the pure white solid product was obtained with 90% yield. ^{1}H NMR (400 MHz, DMSO-d_6): δH 8.30 (2H, s), 7.80 (4H, s); ^{13}C NMR (100 MHz, DMSO-d_6): δC 194.0, 167.9, 134.9, 134.5, 132.4, 128.7, 128.5, ppm. MS HRMS (TOF-ESI): *m/z* calcd: 164.040; found: 164.037 $[M-H]^-$, Δ = 17.0 ppm.

2.4. Synthesis of (3)

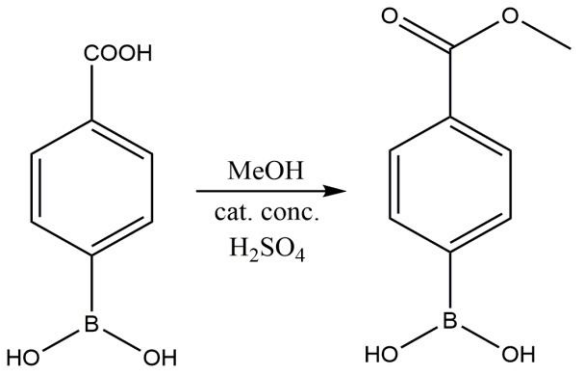

25 mL MeOH was used to dissolve **(2)** (1.0 gr, 6.02 mmol), then 5 drops of concentrated H_2SO_4 was added to the solution of **(2)**. After stirring at reflux for 1 day, the solvent was evaporated under vacuum. Then aqueous Na_2CO_3 was added. The extraction of mixture was carried out by using ethyl acetate and organic phase was washed with water. After the solvent was removed, the pure product (60%) was obtained by recrystallization with toluene. ^{1}H NMR (400 MHz, DMSO-d_6): δH 8.20 (2H, s), 7.80 (4H, s), 3.75 (3H, s); ^{13}C NMR (100 MHz, DMSO-d_6): δC 164.8, 132.6, 129.1, 126.3, 50.4 ppm. MS HRMS (TOF-ESI): *m/z* calcd: 178.056; found: 178.053 $[M-H]^-$, Δ = 13.2 ppm.

2.5. Synthesis of (5)

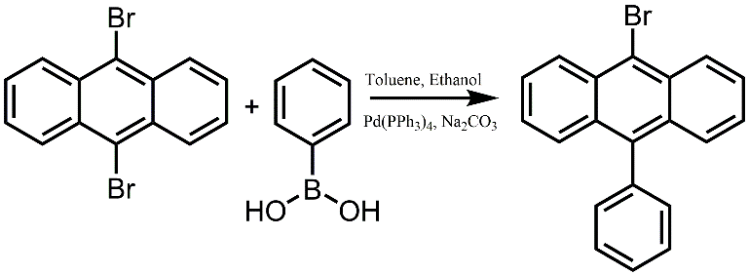

The Suzuki coupling reaction was performed with phenylboronic acid (0.61 g, 5mmol), 9,10-Dibromoanthracene (1.68 g, 5 mmol), $Pd(PPh_3)_4$ (0.58 mg, 0.5mmol) and 2M Na_2CO_3. They were mixed and dissolved in degassed toluene (30 mL), ethanol (10 mL) and distilled water (12 mL). The mixture was stirred for 3 hours at 100 °C. The reaction mixture was extracted with ethyl acetate and the organic phase dried over anhydrous Na_2SO_4. The solvent of organic phase was evaporated under vacuum and compound was purified by silica gel FCC by using hexane as an eluent. The pure white solid was acquired (35%). ^{1}H NMR (400 MHz, $CDCl_3$): δH 8.61 (2H, d, *J* = 8.8 Hz), 7.71-7.62 (2H, m), 7.60-7.53 (5H, m), 7.45-7.30 (4H, m); ^{13}C NMR (100 MHz, $CDCl_3$): δC 138.4, 137.8, 131.1, 131.0, 130.0, 128.4, 127.8, 127.7, 127.4, 126.9, 125.5 ppm. MS HRMS (TOF-ESI): *m/z* calcd: 332.020; found: 332.022 [M], Δ = 5.7 ppm.

2.6. Synthesis of (6)

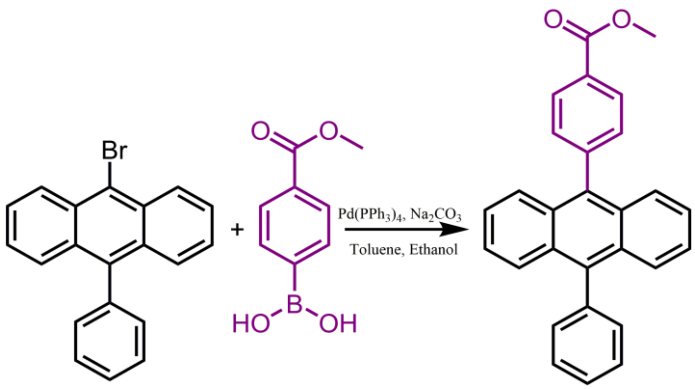

The future Suzuki coupling reaction involved **(3)** (80 mg, 0.44 mmol), **(5)** (150 mg, 0.44 mmol), $Pd(PPh_3)_4$ (61 mg, 0.044 mmol) and 2M Na_2CO_3. They were mixed and dissolved in degassed toluene (6 mL), ethanol (2 mL) and distilled water (3 mL). Reaction was heated for 3 hours at 100 °C. The reaction mixture was extracted with ethyl acetate and the organic phase dried over anhydrous Na_2SO_4. The solvent of organic phase was evaporated under vacuum and compound was purified by silica gel FCC by using 3:1 (DCM: hexane) as an eluent. The pure white solid was acquired (53%). ^{1}H NMR (400 MHz, $CDCl_3$): δH 8.32 (2H, d, *J* = 1.8 Hz), 7.78-7.73 (2H, m), 7.69-7.60 (7H, m), 7.55 (2H, d, *J* = 1.3 Hz), 7.39-7.32 (4H, m), 4.05 (3H, s); ^{13}C NMR (100 MHz, $CDCl_3$): δC 167.1, 144.4, 138.9, 137.8, 135.8, 131.6, 131.5, 131.3, 129.9, 129.7, 129.5, 128.5, 127.6, 127.1, 126.5, 125.4, 125.1, 52.3 ppm. MS HRMS (TOF-ESI): *m/z* calcd: 388.146; found: 388.149 [M], Δ = 6.1 ppm.

2.7. Synthesis of (7)

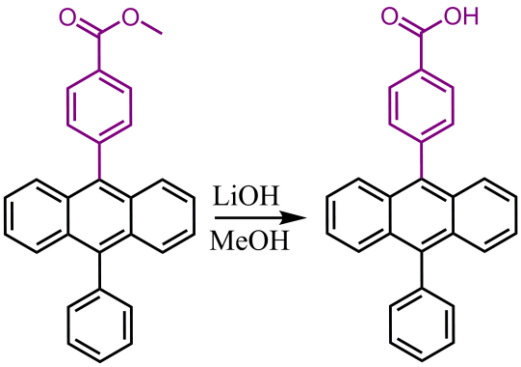

The solution of **(6)** (80 mg, 0.21 mmol) in 5 mL MeOH was mixed with 2M LiOH in 1 mL water. After stirring the mixture for 3 hours at 60 °C, the mixture was acidified to pH 2.0. The precipitate was filtrated and dried (48%). ^{1}H NMR (400 MHz, $CDCl_3$): δH 8.22 (2H, d, *J* = 8.0 Hz), 7.71-7.62 (2H, m), 7.60-7.55 (5H, m), 7.53-7.48 (2H, m), 7.47-7.37 (6H, m); ^{13}C NMR (100 MHz, $CDCl_3$): δC 167.8, 143.5, 138.5, 137.8, 136.1, 131.8, 131.3, 130.7, 130.1, 129.6, 129.4, 129.2, 128.3, 126.9, 126.5, 126.3, 126.0 ppm. MS HRMS (TOF-ESI): *m/z* calcd: 373.123; found: 373.121 $[M-H]^-$, Δ = 5.6 ppm.

2.8. Synthesis of (8)

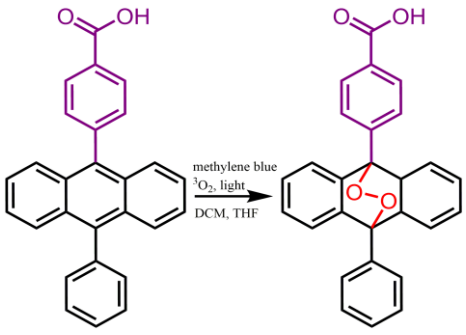

(7) (50 mg, 0.13 mmol) was dissolved in co-solvent DCM-THF (10 mL-5mL) and the solution was cooled to -78 °C. A little amount of methylene blue (0.013 mmol) was added to the solution, then mixture was stirred for 3 hours under O_2 atmosphere. Water cooled 400W Hg arc lamp (white light) irradiation was carried our throughout the reaction. Solvent was evaporated in vacuum and compound was purified by performing silica gel FCC in 95:5 (DCM: MeOH) as an eluent (55%). ^{1}H NMR (400 MHz, $CDCl_3$): δH 8.25 (2H, d, *J* = 1.5 Hz), 7.78 (2H, d, *J* = 1.7 Hz), 7.71 (2H, d, *J* = 1.5 Hz), 7.68-7.59 (3H, m), 7.35-7.29 (4H, m), 7.11-7.02 (4H, m); ^{13}C NMR (100 MHz, $CDCl_3$): δC 140.1, 139.8, 139.5, 132.6, 130.1, 129.1, 128.5, 127.9, 127.5, 127.2, 123.6, 123.4 ppm. MS HRMS (TOF-ESI): *m/z* calcd: 407.129; found: 407.118 $[M-H]^-$, Δ = 25.7 ppm.

2.9. Synthesis of (9)

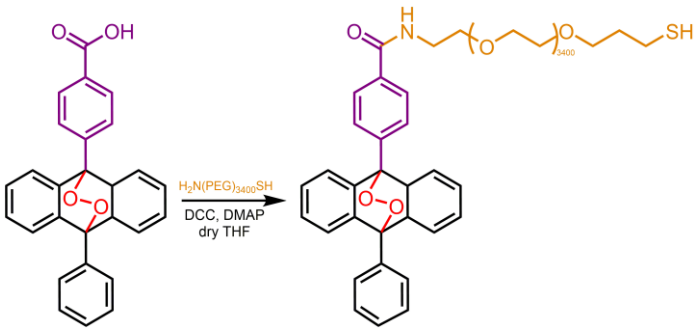

(8) (50 mg, 0.12 mmol), H_2N-PEG-SH (292 mg, 0.086 mmol, MW: 3400 g/mol) were mixed and dissolved in 5 mL dry THF. DCC-DMAP coupling procedure was achieved by the addition of DMAP (11mg, 0.15 mmol) and DCC (26mg, 0.12 mmol) into the solution. The mixture was stirred for 2 hours at room temperature and precipitate

formation was observed. Precipitate was filtered in order to remove side products and cold diethyl ether was added to the solution in order to precipitate the product. After the filtration of the final mixture, the pure white solid product was obtained (42%). ^{1}H NMR (400 MHz, $CDCl_3$): δH 8.12 (2H, d, *J* = 8.2 Hz), 7.78 (2H, d, *J* = 8.2 Hz), 7.71-7.60 (5H, m), 7.21-7.12 (6H, m), 7.11-7.07 (2H, m), 3.78-3.49 (m, PEG), 2.90 (2H, t, *J* = 8.2), 1.22 (2H, s), 0.90 (1H,s). ^{13}C NMR (100 MHz, $CDCl_3$): δC 167.0, 157.2, 140.9, 140.4, 140.1, 139.9, 136.0, 134.5, 132.9, 128.3, 127.7, 127.3, 127.2, 123.5, 123.2, 70.4, 70.3, 70.2, 70.0, 69.9, 69.5, 66.9, 38.5, 33.8, 25.6, 24.9 ppm.

2.10. Synthesis of Gold Nanorod

2.10.1. Preparation of Seed Solution

CTAB solution (5.0 mL, 0.20 M) was mixed with $HAuCl_4$ solution (5.0 mL, 0.00050 M) and the mixture was gently stirred. Then, ice-cold $NaBH_4$ (0.60 mL, 0.010 M) was added that yielded with brownish yellow solution. The mixture was vigorously stirred for 2 min and it was stored at room temperature.

2.10.2. Growth of Gold Nanorods at longitunal LSPR Band

After the preparation of seed solution, CTAB solution (5.0 mL, 0.20 M) was added to $AgNO_3$ solution (0.20 mL, 0.0040 M) at 25 °C. Then, further addition involved $HAuCl_4$ (5.0 mL, 0.0010 M) and they were mixed gently. After a while ascorbic acid

(70.0 μL, 0.0788 M) was added and this addition changed the color of solution from dark yellow to colorless. Final addition contained 12.0 mL of the seed solution to the growth solution at 27-30 °C. During the reaction proceeded, the color change of the solution was observed within 10-20 min. The color of the solution was purple as expected. The temperature of the growth medium was kept at 27-30 °C for 12 hours. The solution was centrifuged at 6000 rpm for 10 min so as to remove excess CTAB solution and the solution dispersed in distilled water. With this seed-mediated growth method, 1.8E+10 nps/mL, 0.060 mg/mL GNRs were obtained.

2.10.3. Decorating of Gold Nanorods with EPOs

In order to acquire effective conjugation between GNRs and EPOs, GNR solution was centrifuged at 14000 rpm for further removal of CTAB. After all excess CTAB solution was removed, equi-volume solutions of **(9)** and GNR (O.D~1.0, ~0.25 nM) were mixed. The mixture was stirred vigorously and sonicated for 1 min. Then, the reaction was left to react for 2 hours. The unreacted **(9)** was removed by centrifugation at 7000 rpm for 10 min and **(9)-GNR** was dispersed in buffer or DMSO.

3. RESULTS & DISCUSSION

Gold nanoparticles with spherical and non-spherical derivatives possess distinctive physicochemical and optical features. The most important parameter for these characteristic properties is the shape of nanoparticles. In regarding to shape of nanoparticles, rod-like gold nanoparticles have been intensely investigating for several applications, such as biological applications, cancer-related therapies, antibacterial therapy, drug releases, bioimaging and so on. The most attractive feature leading to the popularity of gold NRs is its localized surface plasmon resonances (LSPRs) which can be synthetically tuned in order to cover the visible and near-infrared regions of electromagnetic spectrum. In addition to that intriguing feature, photothermal conversion ability of gold nanorods makes them outstanding candidates for photothermal therapy, *hyperthermia*. Thus, the irradiation of gold NRs results in converting light into heat by means of photothermal conversion. Furthermore, easy shape-controlled synthesis methods of gold nanorods give opportunities to produce high yield and quality of nanorods with size controlling. In the light of all these properties of gold nanorods, our project mainly includes the modification of gold nanorods for photodynamic therapy of tumor cells. In our project first synthetic attempt was the production of gold NRs with longitudinal LSPR peak at near-IR region, around 800 nm. As introduced in literature 40 nm gold NRs with aspect ratio of 4 is efficient for our design.[79] So that, with all these physical properties gold NRs was synthesized by applying wet-chemical seed-mediated growth method as reported by El-Sayed procedure.[55] According to that procedure, the reduction of $HAuCl_4$ with sodium borohydride in a surfactant solution yielded with seed solution, containing small gold nanoparticles (1-2 nm). The preferred surfactant of this procedure was

cetyltrimethylammonium bromide, CTAB which governs the longitudinal growth of gold NRs and prevent aggregation of nanocrystals. Then, the overall growth of gold nanorods was performed by step by step reduction of $HAuCl_4$, firstly from Au (III) to Au (I) by ascorbic acid, then from Au (I) to Au (0) by the addition of small amounts of produced seed solution.

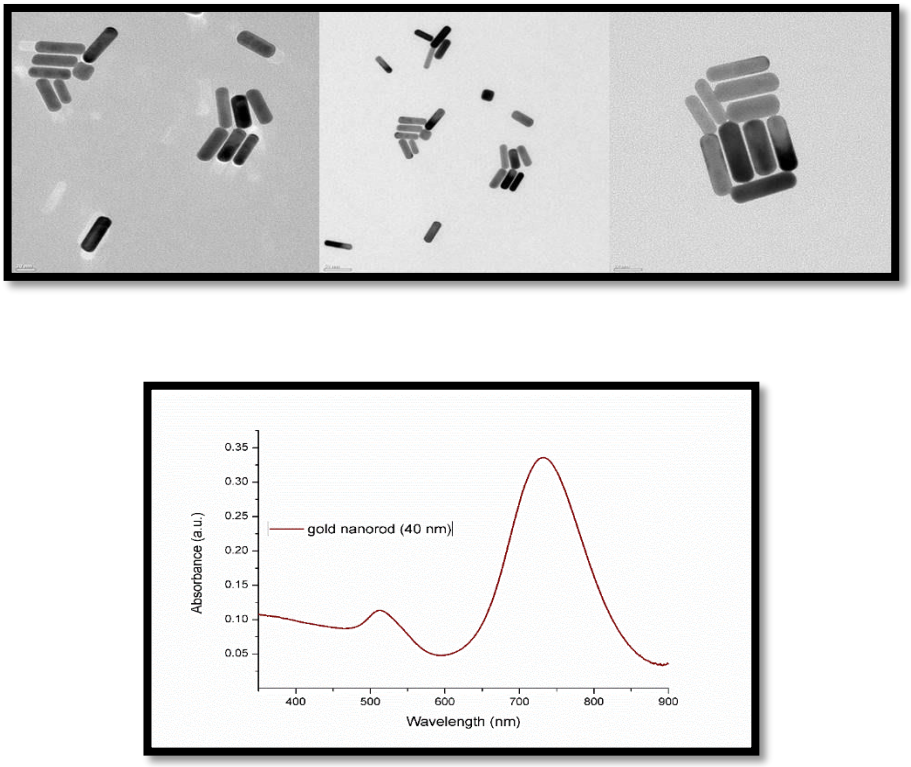

Figure 11.TEM images of gold nanorods (top) and electronic absorption spectrum of gold nanorods in HEPES buffer solution (bottom).

Our synthesized gold NRs was characterized by transmission electron microscopy (TEM) and UV spectroscopy (figure 11). As represented in TEM images (figure 11), highly uniform rod-like shaped nanoparticles with an aspect ratio of 4 were produced successfully. Also, the distinctive longitudinal (the electron oscillation along the length direction) and transverse (the electron oscillation along transverse direction) LSPR peaks of gold NRs were detected by the electronic absorption spectrum (figure

11). Our absorption spectrum represented the transverse peak at around 500 nm and the longitudinal peak at around 800 nm.

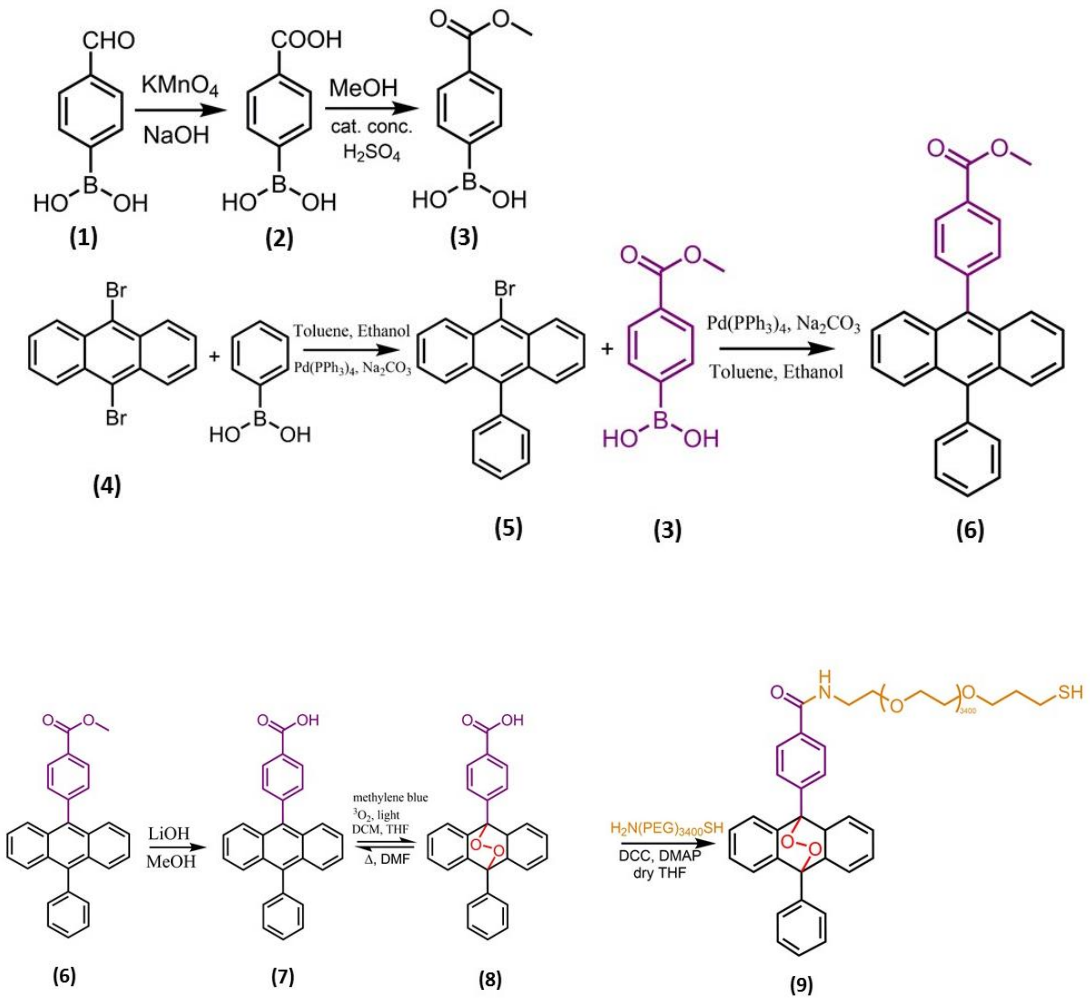

Figure 12. Representation of reaction pathways of our target structure.

With regarding to our project, second synthetic attempt for the conjugation of gold NRs was accomplished by synthesizing a water-soluble anthracenic endoperoxide derivative as represented in figure 12. Our PEGylated anthracenic endoperoxide molecule was synthesized at the end of seven steps reactions. The starting molecule was 4-formylboronic acid and it was oxidized to carboxylic acid in the presence of potassium permanganate, $KMnO_4$. The esterification of this carboxylic acid derivative

was carried out with catalytic amount of concentrated sulfuric acid in MeOH solvent. The formation of methyl ester derivative critical for Suzuki coupling. The reason is that when Suzuki coupling is carried out by 4-carboxypheylboronic acid directly, this carboxylic acid derivative will most probably deactivate the palladium catalyst. The first Suzuki coupling reaction was done between commercial phenylboronic acid and 9, 10-dibromoanthracene. And then further Suzuki coupling was done with mono-substituted anthracenic compound **(5)** and methyl ester derivative of boronic acid **(3)**. The following synthetic pathways contained hydrolysis of ester to acid. This acidification of methyl ester derivative was completed by LiOH after dissolving in MeOH. Before PEGylation of anthracenic molecule, we synthesized the endoperoxide derivative. Our anthracenic molecule **(7)** and methylene blue were dissolved in DCM/ dry THF mixture and then the mixture was irradiated with a water-cooled 400W Hg arc lamp throughout bubbling molecular oxygen, $^{3}O_{2}$. The final reaction for target endoperoxide molecule involved the synthesis of water-soluble thiol-end endoperoxide **(9)**. So that, DCC coupling was achieved between carboxylated anthracenic endoperoxide **(8)** and NH2-$(PEG)_{3400}$-SH in dry THF solvent.

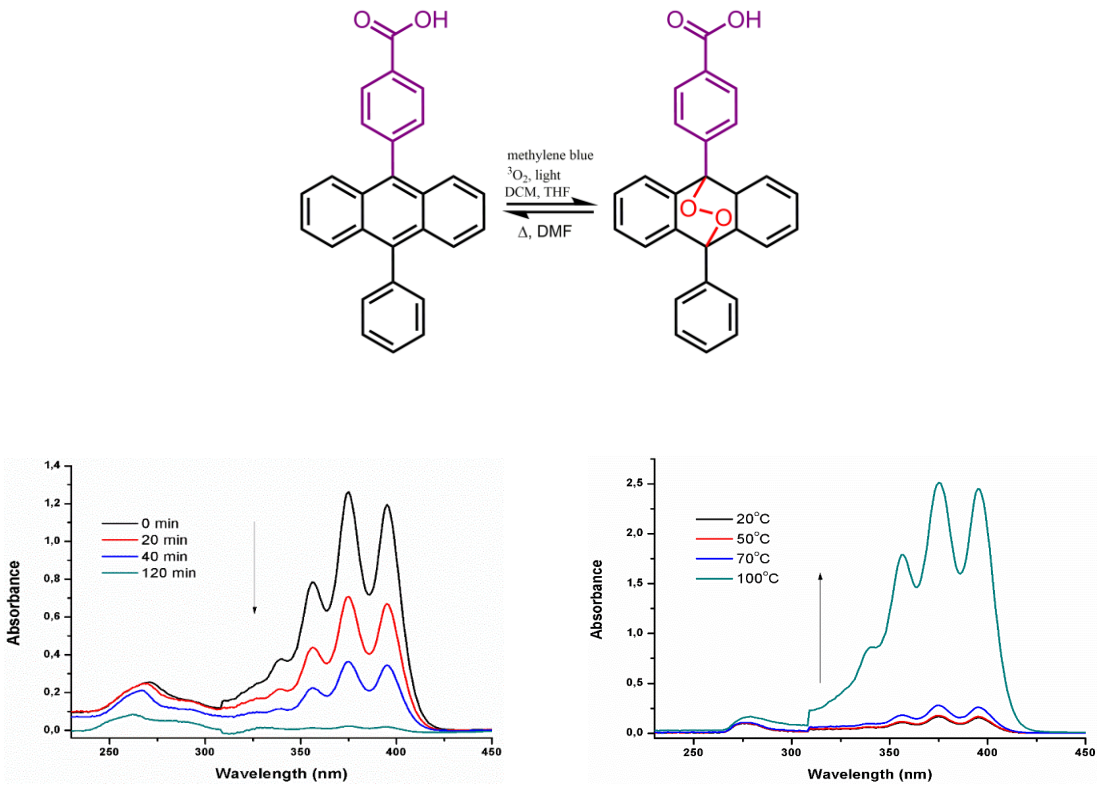

Figure 13. Formation and thermolysis of endoperoxide molecule (8).

Until the endoperoxide formation, all synthesized molecules were characterized by NMR spectroscopy. Yet, in order to detect the endoperoxide formation during the reaction, the electronic absorption spectrum of reaction was also recorded (figure 13, bottom, left). While the reaction proceeds, the typical absorption peaks of the anthracene derivative **(7)** at 352, 375, and 395 nm diminished as observed in figure 13. The reason of that decrease in absorbance was the disruption of aromaticity due to the reaction between the parent anthracene and $^1O_2$ that represents the typical [4+2] cycloaddition reaction. Under -78°C condition the reaction was terminated at the end of two hours, afterwards no absorbance peaks of parent anthracene were obtained. Nevertheless, as shown in figure 13 we also controlled the reappearance of absorbance peaks of parent anthracene by reinstating the aromaticity (figure 13, bottom, right). So that, heating the endoperoxide molecule in DMF solution resulted in the release of

oxygen and reappearance of typical absorbance bands of anthracene regarding to thermal decomposition of endoperoxide molecule **(8)**.

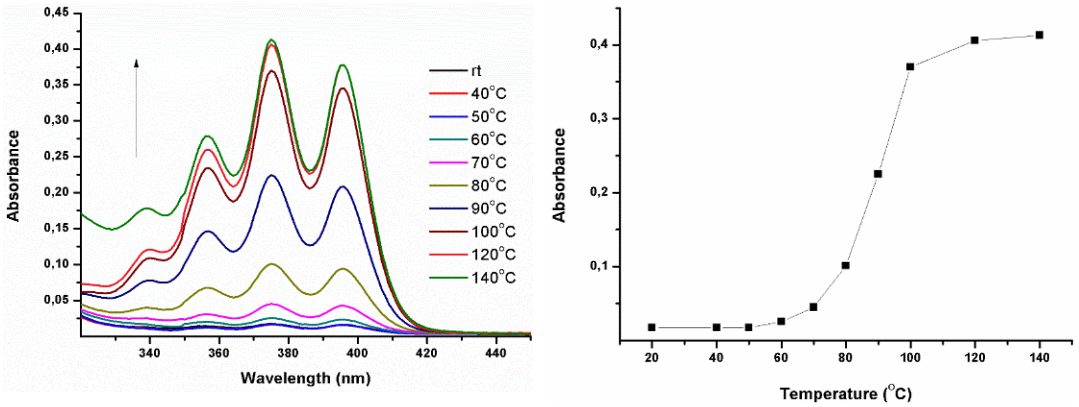

Figure 14.Left: Thermolysis of 5x10-5 M PEGylated endoperoxide molecule (9) in DMSO at various temperature. Right: Thermolysis of (9) represented as absorbance vs. temperature graph. For all selected temperatures the reaction was heated for 30 min.

Further investigation involved thermal decomposition of our PEGylated endoperoxide compound **(9)** in order to show reinstating the aromaticity upon heating the target molecule. In this manner, our target molecule has been heated for 1 hour for each selected temperatures in DMSO solution. Figure 14 represented expected reappearance of typical absorbance peaks of parent anthracene compound in the order of 352, 375, and 395 nm. The thermal decomposition of our compound **(9)** was completed at the end of 9 hours at 140°C (figure 14). Furthermore, in our design the most critical condition is whether our target molecule **(9)** is going to decompose at body temperature (37°C) or not. For that purpose, compound **(9)** was heated at 95 °C and 37°C for six hours (figure 15). Thus, even if efficient thermolysis observed at 95 °C, heating **(9)** at 37°C could not lead to anthracene absorption. According to these measurements, our target molecule can be used under physiological condition without any destruction to body.

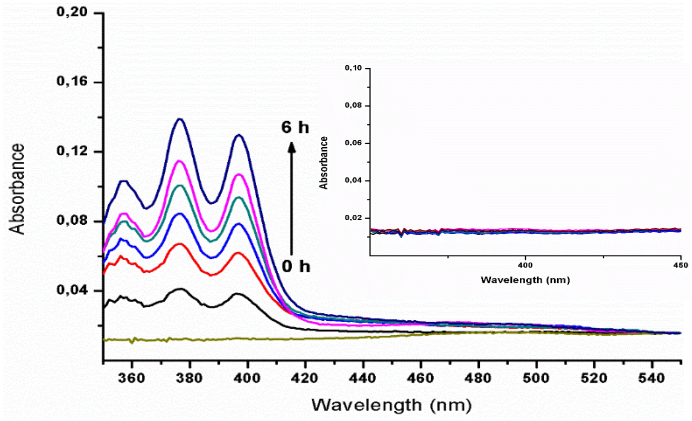

Figure 15.Thermolysis of 5x10-5 M PEGylated endoperoxide molecule (9) in DMSO at 95ºC for 6 hours. Inset: Absorbance of 5x10-5 M (9) in DMSO at 37ºC and again the molecule was heated for 6 hours at body temperature.

Regarding to cell culture studies of our design, thermal decomposition of compound **(9)** in aqueous medium is crucial. The oxygen release experiment from **(9)** was studied by heating molecule in double-distilled water in a closed system. So that, heating at 100°C for 1 hour resulted in the reappearance of absorbance bands of parent anthracene as observed in organic solvents (figure 16).

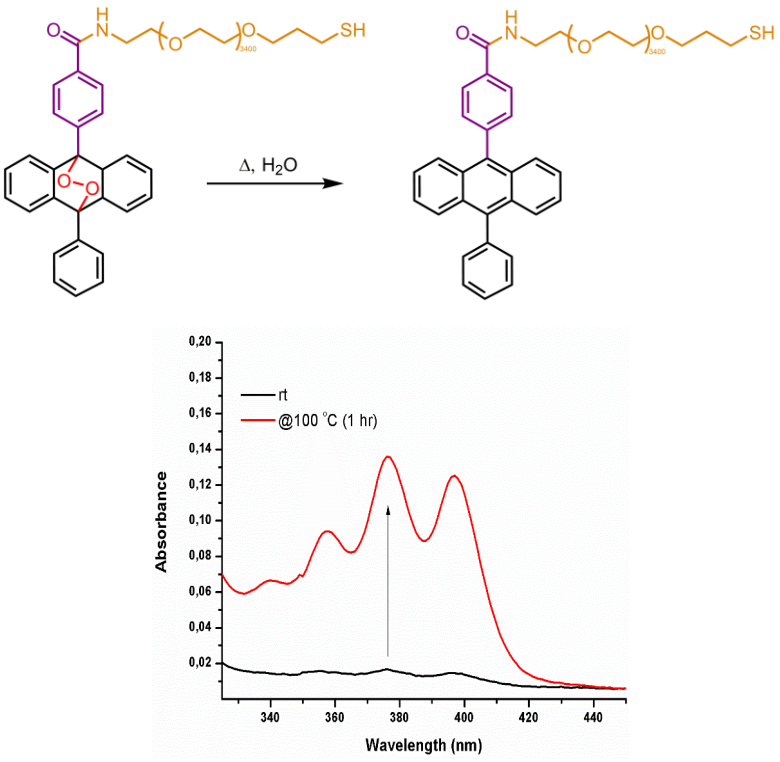

Figure 16.Thermolysis of 1x10-5 M PEGylated endoperoxide molecule (9) in HEPES buffer (pH 7.2, 20 mM) at 100oC for 1 hr.

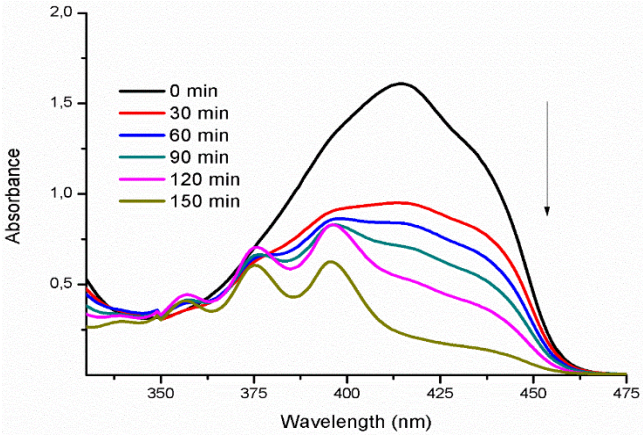

Figure 17. The results related to the decomposition of trap molecule (DPBF) owing to existence of singlet oxygen.

The thermal decomposition results showed that our target molecule **(9)** was considered as an appropriate compound for the oxygen release studies. As introduced in literature,

polycyclic aromatic endoperoxides are very good candidate for releasing both molecular ($^3O_2$) and singlet oxygen ($^1O_2$) upon heating.[45] According to this information the existence of singlet oxygen after thermolysis of endoperoxide compound should be demonstrated. So that, we used diphenyl*iso*benzofuran (DPBF) as a singlet oxygen trap molecule. In the case of existence of $^1O_2$, the trap molecule reacts with oxygen and it undergoes to decomposition of molecular structure that leads to decrease in absorbance band at 414 nm (figure 17). In this way, $1x10^{-5}$ M **(9)** was mixed with DPBF after the absorbance of this trap molecule was arranged to around O.D~1, then we heated the mixture at 70°C for 150 minutes. The electronic absorption spectra of little amount of mixture was recorded in every 30 minutes. As represented in figure 17, the first dramatic decrease in DPBF absorption after 30 minute substantiated the generation of singlet oxygen. The absorption spectrum of the mixture for 120 minute indicated the reappearance of absorbance bands of anthracene compound. At the end of 150 minutes the decomposition of trap molecule because of production of singlet oxygen was observed (figure 17).

After all expected results associated with the compound **(9)** acquired, we conjugated PEGylated endoperoxide molecule **(9)** with gold NRs. The conjugation was described by TEM images of gold NRs and further characterization was done with UV spectroscopy (figure 18). The electronic absorption spectrum of conjugated gold NRs represented the red shifted LSPR maximum of nanorods both in buffer and DMSO, respectively.

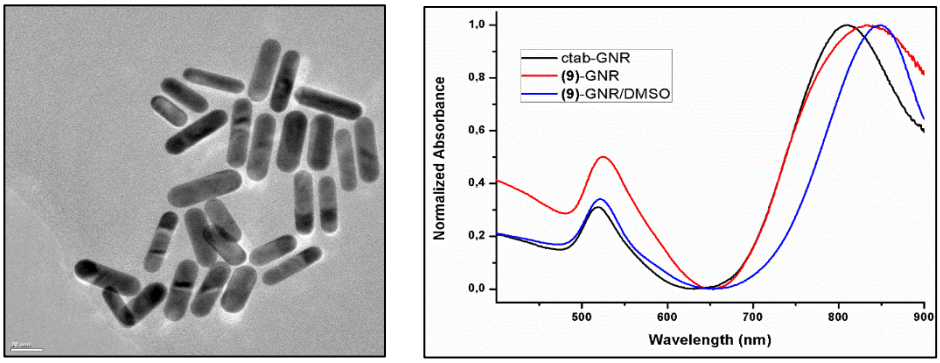

Figure 18. Left: TEM image after the conjugation of PEGylated endoperoxide (9) with gold NRs. Right: Normalized electronic absorption spectra of CTAB-GNR, (9)-GNR (in HEPES (pH 7.2, 20 mM) and (9)-GNR in DMSO.

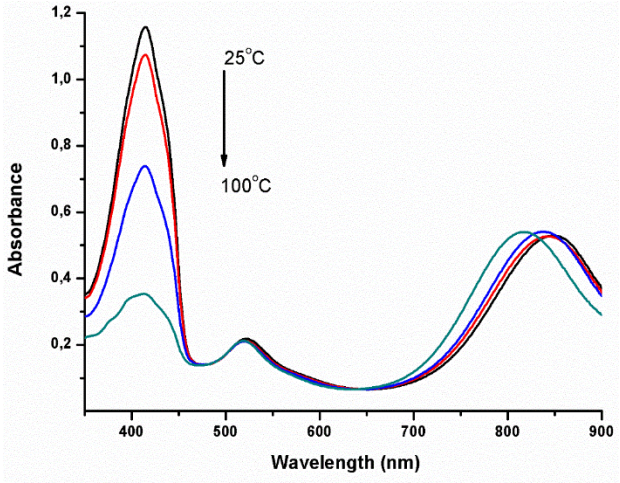

Figure 19. Heating 1x10-5 M GNR-(9) conjugate at 70 ◦C in DMSO resulted in the absorbance decrease of DPBF.

Furthermore, the presence of singlet oxygen after conjugation of gold NRs and the compound **(9)** was also proved by heating the mixture which contained trap molecule. The electronic absorption spectra of the mixture represented that the expected generation of singlet oxygen leaded to decrease in absorption of trap molecule as temperature increased (figure 19). After obtaining promising results in oil bath, the singlet oxygen generation experiments associated with the conjugate molecule (**(9)**-gold NRs) was conducted via laser irradiation. For that studies, the gold nanorod-**(9)**

conjugate (**GNR-(9)**) was mixed with singlet oxygen trap molecule and the mixture was dispersed in DMSO, then it was irradiated by 830 nm laser light. As represented in figure 20, the electronic absorption spectra of DPBF decreased as a result of singlet oxygen generation. In that experiment, the irradiation of gold NRs leads to local temperature increase on the surface of nanorods by virtue of the excitation of its longitudinal LSPR peak (830 nm). This excitation activates the thermolysis of **(9)** which was conjugated to gold NRs. However, no decrease in the absorption of trap molecule was observed, when the solution which contained gold nanorods without any conjugation was irradiated with laser light (figure 21). The relative $^1O_2$ efficiency of unconjugated GNR and GNR-**(9)** was demonstrated as absorbance vs. time graph in figure 22.

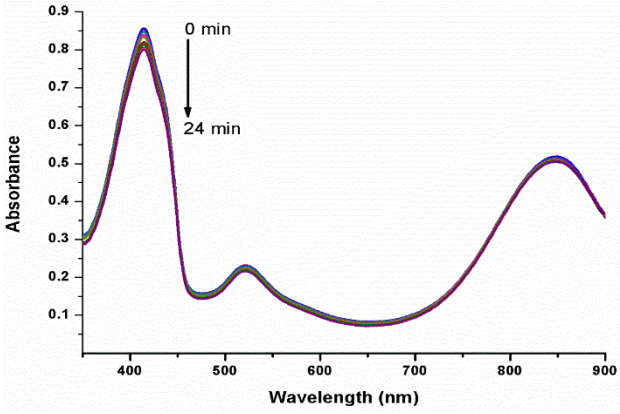

Figure 20. The irradiation of gold NR-(9) with the laser at 830 nm resulted in the decrease of absorbance maximum of DPBF at 414 nm.

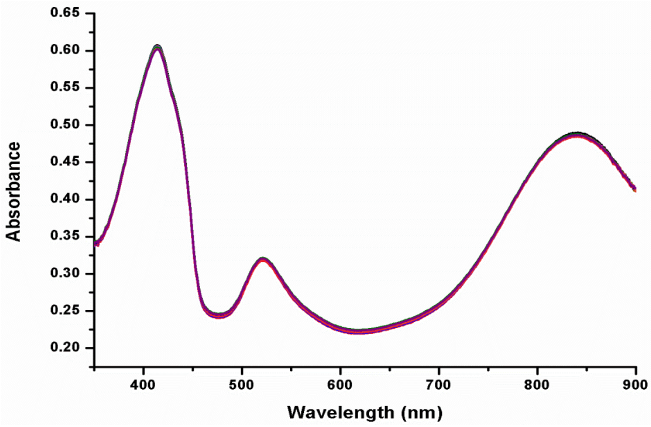

Figure 21. The effect of unconjugated GNRs on the absorbance of DPBF after excition with 830 nm laser light.

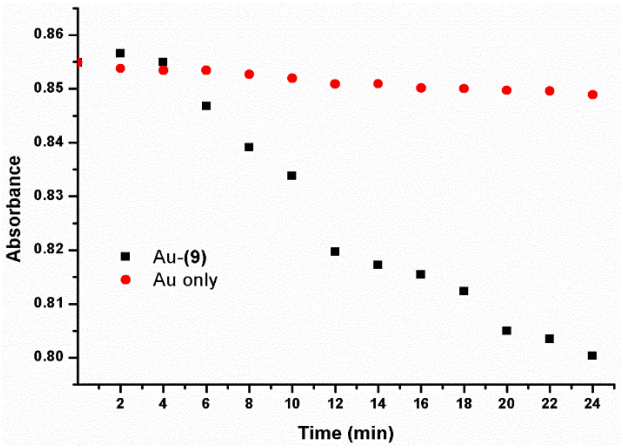

Figure 22. The differences in the singlet oxygen yield of GNR and GNR-(9) conjugate in DMSO.

In vivo studies of our GNR-(9) conjugate was performed with the collaboration of Yoon et al. They used HeLa cancer cell which is commonly used cervical type cancer cells. Before performing in vivo studies, we synthesized unconjugated GNRs, GNR-(9) conjugates and GNR-PEG molecules. The reason of the synthesis of GNR-PEG was that the toxicity of unconjugated GNR can be removed by any modification of gold nanoparticles. So that, we pegylated GNR particles by using DCC-DMAP coupling in the presence of benzoic acid and H_2N-PEG-SH. First study involved the

cell images with confocal microscopy in order to represent the effects of ROS sensor (figure 23). HeLa cells were incubated with unconjugated GNR, GNR-PEG, GNR-(9) and GNR-(9) in the presence of NaN_3. After incubation process, they were irradiated with 808 nm laser light for 10 minute. Figure 23 demonstrated that Hela cells were painted by ROS sensors due to the singlet oxygen generation after irradiaton of GNR-(9). As represented in the first row of figure 23, ROS sensors can be active only in the case of the existence of cytotoxic singlet oxygen. At the same time, the study showed that unconjugated GNRs and GNR-PEG conjugates did not produce singlet oxygen. Furthermore, the cytotoxic singlet oxygen species were quenched in a large extend because of the presence of NaN_3 (figure 23, top, d), so ROS sensor could not react with all generated singlet oxygen. In the following figure 24, the acquired cell images represented the selectively apoptotic cell death. All Hela cells were incubated with unconjugated GNR (a), GNR-PEG (b), GNR-(9) (c) and GNR-(9) in the presence of NaN_3 (d), then all cells were incubated with 808 nm laser for 10 min and incubated for 16 hr and stained with Annexin V. Annexin V is used as an apoptosis marker in cell culture studies. Figure 24, c showed that HeLa cells were killed by cytotoxic singlet oxygen after irradiation of GNR-(9) complexes.

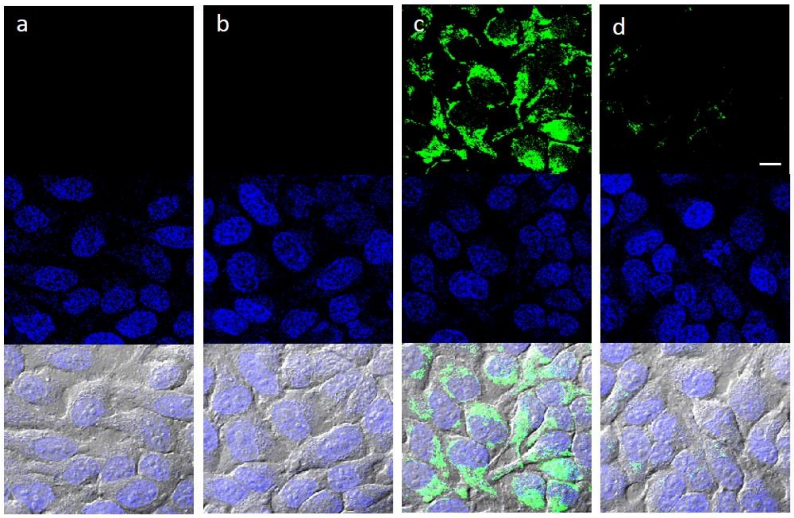

Figure 23. The confocal microscopy of HeLa cells represented ROS generation (top: ROS sensor, middle: DAPI, bottom: merged with DIC).

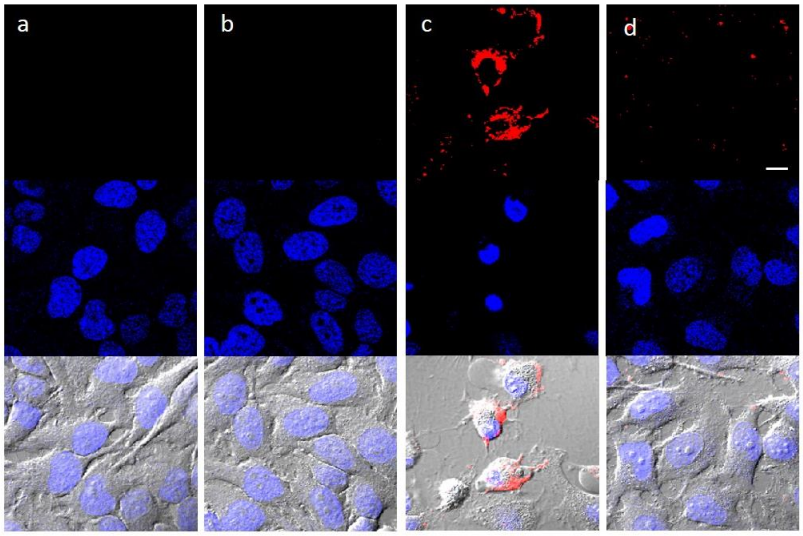

Figure 24. The confocal microscopy of HeLa cells represented apoptotic cell death by Annexin V (top: Annexin V, middle: DAPI, bottom: merged with DIC).

The final study involved the MTT assay for Hela cell's viability. Hela cells were incubated with 10 pM GNR, GNR-PEG, GNR-(9) for 24 hr and then they were irradiated with 808 nm laser. Figure 25 represented the dramatic death of Hela cells

due to the generation of cytotoxic singlet oxygen in the presence of GNR-(9) conjugates.

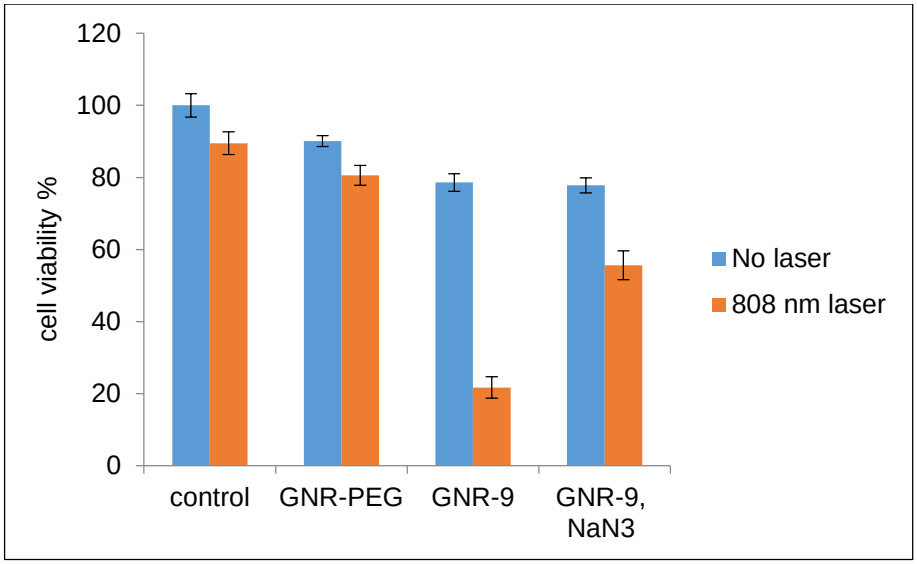

Figure 25. Hela cell's viability was assayed by MTT test after irradiation with 808 nm laser (2 W/cm^2 , 10 min).

4. CONCLUSION

In this study, we focused on the major problems of PDT that prevent the spread of this therapeutic action through clinical application. The two major problems are hypoxia (molecular oxygen deficiency in tumor tissues) and light penetration depth through tissues. In order to handle with these problems, we described the new approach by combining watersoluble anthracenic endoperoxide derivative with near-IR absorbing gold nanorods. Irradiation of gold nanorods results in the temperature increase on the surface of the nanorods which has a positive effect on hyperthermia. However, in this project heating itself is not primary goal of the therapeutic action, but it is used as a triggering agent for singlet oxygen. At that point the generation of singlet oxygen leads to bring up against hypoxia. As discussed previously, the singlet oxygen generation consumes the molecular oxygen in tumor tissues very fast that leads to molecular oxygen deficiency in that tissues. Therefore, during the process of generating singlet oxygen, the dose of irradiation has to be fine-tuned. Furthermore, the thermal decomposition of endoperoxides results in either singlet oxygen ($^1O_2$) or triplet molecular oxygen ($^3O_2$). During this thesis process, singlet oxygen trap experiments by applying laser light demonstrated the efficiency of singlet oxygen yield of our GNR-(9) conjugate.

The interdisciplinary feature of PDT inspires us to design a promising molecular structure by combining organic chemistry with nanoparticles. Thus, in this thesis, we tried to present a new anti-tumor molecule to handle with the challenges of PDT.

REFERENCES

1. Dolmans, D. E. J. G. J.; Fukumura, D.; Jain, R. K. Photodynamic therapy for cancer. *Nat. Rev. Cancer* **2003**, *3*, 380–387.

2. Spikes, J. D.: *Primary Photoprocesses in Biology and Medicine*; Plenum Press: New York, **1985**.

3. Huang, Z. A review of progress in clinical photodynamic therapy. *Technol. Cancer Res. Treat.* **2005**, *4*, 283–293.

4. Sharman, W. M.; Allen, C. M.; Lier, J. E. Photodynamic therapeutics : basic principles and clinical applications. *Elsevier Science.* **1999**, *4***,** 507–517.

5. Verlag, F. The Modes of Cell Death Induced by PDT : An Overview. *Med. Laser Appl.* **2003**, *19*, 7–19.

6. Kubler, A. C. Photodynamic therapy. *Med. Laser Appl.* **2005**, *20*, 37–45.

7. Daniell, M. D.; Hill, J. S. A HISTORY OF PHOTODYNAMIC THERAPY. *Aust. Nz. J. Surg.* **1991**, *61***,** 340–348.

8. Ackroyd, R.; Kelty, C.; Brown, N.; Reed, M. The History of Photodetection and Photodynamic Therapy. *Photochem. Photobiol.* **2001**, *74*, 656–669.

9. Carvin, J. F.: *Des Bienfaits de L'insolation*; Paris, **1815**.

10. Allison R. R.; Mota H.C.; Sibata C. H. Clinical PD/PDT in North America: an historical review. *Photodiagnosis Photodyn Ther.* **2004**, *1***,** 263–277.

11. Raab, O. Uber die Wirkung fluoreszierender Stoffe auf Infusorien. *Zeitung Biol.* **1900**, *39*, 524–526.

12. Von Tappeiner, H. Ueber die wirkung fluorescierenden stoffe auf infusiorien nach versuchen von O Raab. *Munch Med Wochenschr* **1900**, *47*.

13. Von Tappeiner, H.; Jodlbauer, A.: *Die Sensibilisierende Wirkung Fluorescierender Substanzer. Untersuchungen Uber die Photodynamische Erscheinung*; Vogel, F.C.: Leipzig, **1907**.

14. Von Tappeiner, H.; Jesionek, A. Therapeutische Versuche mit fluorescierenden Stoffen. *Munch. Med. Wochenschr* **1903**, *47*, 2042–2044.

15. Jesionek, A.; von Tappeiner, H. Zur behandlung der Hautcarcinome mit fluorescierenden Stoffen. *Arch. Klin. Med.* **1905**, *82*, 223.

16. Finsen, N. R. *Phototherapy*; Edward Arnold: London, **1901**.

17. Scherer, H. Chemical-physiological investigations. *Ann. D. Chem. Pharm.* **1841,** *40*, 1–64.

18. Hausmann, W. Die sensibilisierende Wirkung des hamatoporphyrins. *Biochem. Z.* **1911**, 276–316.

19. Meyer-Betz, F. Untersuchungen uber die Biologische (photodynamische) Wirkung des hamatoporphyrins und anderer Derivative des Blut-und Gallenfarbstoffs. *Dtsch. Arch. Klin. Med.* **1913**, *112*, 476–503.

20. Lipson, L. R.; Baldes, E. J. The photodynamic properties of a particular haematoporphyrin derivative. *Arch. Dermatol.* **1960**, *82*, 508–516.

21. Lipson, L. R.; Baldes, E. J.; Olsen, A. M. The use of a derivative of haematoporphyrin in tumor detection. *J. Natl. Cancer Inst.* **1961,** *26*, 1–11.

22. Lipson, L. R.; Baldes, E. J.; Olsen, A. M. Hematoporphyrin derivative: A new aid for endoscopic detection of malignant disease. *J. Thorac. Cardiovasc. Surg.* **1961,** *42*, 623–629.

23. Lipson, L. R.; Baldes, E. J.; Gray, M. J. Hematoporphyrin derivative for detection and management of cancer. *Cancer* **1967,** *20*, 2255–2257.

24. Diamond, I. Photodynamic therapy of malignant tumours. *Lancet* **1972**, *2*, 1175–1177.

25. Dougherty, T. J.; Grindey, G. B.; Fiel, R.; Weishaupt, K. R.; Boyle, D. G. Photoradiation therapy. II. Cure of animal tumors with hematoporphyrin and light. *J. Natl. Cancer Inst.* **55,** 115–121 (1975).

26. Kelly, J. F. & Snell, M. E. Hematoporphyrin derivative: a possible aid in the diagnosis and therapy of carcinoma of the bladder. *J. Urol.***1976**, *115*, 150–151.

27. Dougherty, T. J. Photoradiation Therapy for the Treatment of Malignant Tumors Photoradiation Therapy for the Treatment of Malignant Tumors. *Cancer Res.* **1978**, *38*, 2628–2635.

28. Balchum, O. J.; Doiron, D. R.; Huth, G. C. Photoradiation therapy of endobronchial lung cancers employing the photodynamic action of hematoporphyrin derivative. *Lasers Surg. Med.* **1984,** *4*, 13–30.

29. McCaughan, J. S.; Jr, Hicks, W.; Laufman, L.; May, E.; Roach, R. Palliation of Esophageal Malignancy With Photoradiation Therapy. *Cancer* **1984**, *54*, 2905-2910.

30. Dimofte, A.; Zhu, T. C.; Hahn, S. M.; Lustig, R. A. In vivo light dosimetry for motexafin lutetium-mediated PDT of breast cancer. *Lasers Surg. Med.* **2002,** *31*, 305–312.

31. Schweitzer, V. G. Photodynamic therapy for treatment of head and neck cancer. *Otolaryngol. Head Neck Surg.* **1990**, *102*, 225–232.

32. Bown, S. G.; Rogowska, A. Z.; Whitelaw, D. E.; Lees, W. R.; Lovat, L. B.; Ripley, P.; Jones, L.; Wyld, P.; Gillams, A.; Hatfield, A. W. R. Photodynamic therapy for cancer of the pancreas. *Gut* **2002**, *50*, 549–557.

33. Hornung, R. Photomedical approaches for the diagnosis and treatment of gynecologic cancers. *Curr. Drug Targets Immune Endocr. Metabol. Disord.* **2001**, *1*, 165–177.

34. Sandeman, D. R. Photodynamic therapy in the management of malignant gliomas: a review. *Lasers Med. Sci.***1986**, *1*, 163–167.

35. Kennedy, J. C.; Pottier, R. H.; Pross, D. C. Photodynamic therapy with endogenous protoporphyrin IX: basic principles and present clinical experience. *J. Photochem. Photobiol. B.* **1990,** *6*, 143–148.

36. Agostinis, P.; Berg, K.; Cengel, K. A.; Foster, T. H.; Girotti, A. W.; Gollnick, S. O.; Hahn, S. M.; Hamblin, M. R.; Juzeniene, A.; Kessel, D.; Korbelik, M.; Moan, J.; Mroz, P.; Nowis, D.; Piette, J.; Wilson, B. C.; Golab, J. Photodynamic Therapy of Cancer : An Update. *Am. Cancer Soc.* **2011**, *61*, 250–281.

37. Brancaleon, L.; Moseley, H. Laser and Non-laser Light Sources for Photodynamic Therapy. *Lasers Med. Sci.* **2002,** *17*, 173–186.

38. Sibata, C. H.; Colussi, V. C.; Oleinick, N. L.; Kinsella, T. J. Photodynamic therapy in oncology. *Expert Opin Pharmacother* **2001,** *2*, 917–927.

39. Juzeniene, A.; Nielsen, K. P.; Moan, J. Biophysical aspects of photodynamic therapy. *J. Environ. Pathol. Tox.* **2006**, *25*, 7–28.

40. Turro, N. J.; Ramamurthy, V.; Scaiano, J. C. *Principles of Molecular Photochemistry: An Introduction*; University Science Books: Sausalito, **2009**.

41. Zhao, J.; Wu, W.; Sun, J.; Guo, S. Triplet photosensitizers : from molecular design for applications. *Chem. Soc. Rev.* **2013**, *42*, 5323–5351.

42. Lakowicz, J. R. *Principles of Fluorescence Spectroscopy*; Academic/Plenum, **1999**.

43. Moan, J.; Berg, K.; Kvam, E.; Western, A.; Malik, Z.; Rück, A.; Schneckenburger, H. Intracellular localization of photosensitizers. *Ciba Found Symp.* **1989**, *146*, 95–107.

44. Henderson, B. W.; Waldow, S. M.; Mang, T. S.; Potter, W. R.; Malone, P. B.; Dougherty, T. J. Tumor Destruction and Kinetics of Tumor Cell Death in Two Experimental Mouse Tumors following Photodynamic Therapy. *Cancer* **1985,** *45*, 572–576.

45. Korbelik, M.; Krosl, G. Cellular levels of photosensitisers in tumours : the role of proximity to the blood supply. *Br. J. Cancer* **1994**, *80*, 604–610.

46. Korbelik, M. Induction of tumor immunity by photodynamic therapy. *J. Clin. Laser Med. Surg.* **1996,** *14***,** 329–334.

47. Tromberg, B. J.; Orenstein, A.; Kimel, S.; Barker, S. J.; Hyatt, J.; Nelson, J. S.; Berns, M. W. Invivo Tumor Oxygen-Tension Measurements for the Evaluation of the Efficiency of Photodynamic Therapy. *Photochem. Photobiol.* **1990**, *52*, 375–385.

48. Henderson, B. W.; Fingar, V. H. Oxygen Limitation of Direct Tumor180 Cell Kill during Photodynamic Treatment of a Murine Tumor-Model. *Photochem. Photobiol.* **1989**, *49*, 299–304.

49. Ferrario, A.; von Tiehl, K. F.; Rucker, N.; Schwarz, M. A.; Gill, P. S.; Gomer, C. J. Advances in Brief Antiangiogenic Treatment Enhances Photodynamic Therapy Responsiveness in a Mouse Mammary Carcinoma. *Cancer Res.* **2000**, *60*, 4066–4069.

50. Henderson, W.; Dougherty, J. HOW DOES PHOTODYNAMIC THERAPY WORK ? *Photochem. Photobiol.* **1992**, *55*, 145–157.

51. Shumaker, B. P.; Hetzel, F. W. Clinical laser photodynamic therapy in the treatment of bladder carcinoma. *Photochem. Photobiol.* **2002**, *46*, 899–901.

52. de Vree, W. J. A.; Essers, M. A.; de Bruijn, H. S.; Star, W. M.; Koster, J. F.; Sluiter, W. Evidence for an Important Role of Neutrophils in the Efficacy of Photodynamic Therapy *in Vivo. Cancer Research* **1996**, *56*, 2908–2912.

53. Tolochko, N. K. *History of nanotechnology*; EOLSS, **2007**.

54. Chen, H.; Shao, L.; Li, Q.; Wang, J. Gold nanorods and their plasmonic properties. *Chem. Soc. Rev.* **2013**, *42*, 2679-2724.

55. Narayanan, R.; El-Sayed, M. A. Catalysis with transition metal nanoparticles in colloidal solution: nanoparticle shape dependence and stability. *J. Phys. Chem. C* **2005**, *109*, 12663–12676.

56. Huang, B. X.; Neretina, S.; El-sayed, M. A. Gold Nanorods : From Synthesis and Properties to Biological and Biomedical Applications. *Adv. Mater.***2009**, *21*, 4880–4910.

57. Garcı, F. J.; Abajo, D. Nonlocal Effects in the Plasmons of Strongly Interacting Nanoparticles , Dimers , and Waveguides. *J. Am. Chem. Soc.* **2008**, *112*, 17983-17987.

58. Vigderman, L.; Khanal, B. P.; Zubarev, E. R. Functional Gold Nanorods : Synthesis , Self-Assembly , and Sensing Applications. *Adv. Mater.***2012**, *24*, 4811–4841.

59. Lohse, S. E.; Murphy, C. J. The Quest for Shape Control : A History of Gold Nanorod Synthesis. *Chem. Mater.* **2013**, *25*, 1250-1261.

60. Link, S.; El-sayed, M. A. Spectral Properties and Relaxation Dynamics of Surface Plasmon Electronic Oscillations. *J. Phys. Chem. B* **1999**, *103*, 8410–8426.

61. Ali, M. R. K.; Snyder, B.; El-sayed, M. A. Synthesis and Optical Properties of Small Au Nanorods Using a Seedless Growth Technique. *Langmiur* **2012**, *28*, 9807-9815.

62. Dreaden, E. C.; Alkilany, A. M.; Huang, X.; Murphy, C. J.; El-Sayed, M. A. The golden age: gold nanoparticles for biomedicine. *Chem. Soc. Rev.* **2012,** *41*, 2740-2779.

63. Jain, P. K.; Lee, K. S.; El-sayed, I. H.; El-sayed, M. A. Calculated Absorption and Scattering Properties of Gold Nanoparticles of Different Size , Shape , and Composition : Applications in Biological Imaging and Biomedicine. *J. Phys. Chem. B* **2006**, *110*, 7238–7248.

64. Chen, H.; Shao, L.; Ming, T.; Sun, Z.; Zhao, C.; Yang, B.; Wang, J. Understanding the Photothermal Conversion Effi ciency of Gold Nanocrystals. *small* **2010**, *6*, 2272–2280.

65. Choi, C. H. J.; Alabi, C.; Webster, P.; Davis, M. E. Mechanism of active targeting in solid tumors with transferrin-containing gold nanoparticles. *Proc. Natl. Acad. Sci. U. S. A.* **2010**, *107*, 1235–1240.

66. Huang, Y. F.; Sefah, K.; Bamrungsap, S.; Chang, H. T.; Tan, W. *Langmuir* **2008**, *24*, 11860–11865.

67. Baffou, G.; Kreuzer, M. P.; Kulzer, F.; Quidant, R. Temperature mapping near plasmonic nanostructures using fluorescence polarization anisotropy. *Opt. Express* **2009,** *17*, 3291–3298.

68. Baffou, G.; Girard, C.; Quidant, R. Mapping Heat Origin in Plasmonic Structures. *PRL.* **2010**, *104*, 136805 (1–4).

69. Faraday, M.: *Philos. Trans. R. Soc.;* London, **1857**.

70. Pérez-Juste, J.; Pastoriza-Santos, I.; Liz-Marzán, L. M.; Mulvaney, P. Gold nanorods: Synthesis, characterization and applications. *Coord. Chem. Rev.* **2005**, *249*, 1870–1901.

71. Ye, X. C.; Jin, L. H.; Caglayan, H.; Chen, J.; Xing, G. Z.; Zheng, C.; Doan-Nguyen, V.; Kang, Y. J.; Engheta, N.; Kagan, C. R.; Murray, C. B. *ACS Nano* **2012**, *6*, 2084.

72. Esumi, K.; Matsuhisa, K.; Torigoe, K. No Title. Preparation of rodlike gold particles by UV irradiation using cationic micelles as a template. *Langmuir* **1995**, *11*, 3285-3287.

73. Chang, S.S.; Shih, C.W.; Chen, C.D.; Lai, W.C.; Wang, C. R. C. The Shape Transition of Gold Nanorods. *Langmuir* **1999**, *15*, 701–709.

74. Cao, J. M.; Ma, X. C.; Zheng, M. B.; Liu, J. S.; Ji, H. M. No Title. *Chem. Lett.* **2005**, *24*, 730.

75. Okitsu, K.; Sharyo, K.; Nishimura, R. One-Pot Synthesis of Gold Nanorods by Ultrasonic Irradiation : The Effect of pH on the Shape of the Gold Nanorods and Nanoparticles. *Langmuir* **2009**, *25*, 7786–7790.

76. Masuda, H.; Tanaka, H.; Baba, N. *Chem. Lett.* **1990**, 621.

77. Jana, N. R.; Geartheart, L.; Murphy, C. J. Seed-Mediated Growth Approach for Shape- Controlled Synthesis of Spheroidal and Rod-like Gold Nanoparticles Using a Surfactant Template. *Adv. Mater.***2001**, *13*, 1389–1393.

78. Gole, A.; Murphy, C. J. Seed-Mediated Synthesis of Gold Nanorods : Role of the Size and Nature of the Seed. *Chem. Mater.* **2004**, *16*, 3633–3640.

79. Nikoobakht, B.; El-sayed, M. A. Preparation and Growth Mechanism of Gold Nanorods (NRs) Using Seed-Mediated Growth Method. *Chem. Mater.* **2003**, *15*, 1957–1962.

80. Busbee, B. D.; Obare, S. O.; Murphy, C. J. An Improved Synthesis of High-Aspect-Ratio Gold Nanorods. *Adv. Mater.* **2003**, *15*, 414-416.

81. Liu, M.; Guyot-sionnest, P. Mechanism of Silver (I) -Assisted Growth of Gold Nanorods and Bipyramids. *J. Phys. Chem. B* **2005**, *109*, 22192–22200.

82. Murphy, C. J.; Sau, T. K.; Gole, A.; Orendorff, C. J.; Gao, J.; Gou, L.; Hunyadi, S. Li, T. Anisotropic Metal Nanoparticles: Synthesis, Assembly, and Optical Applications. *J. Phys. Chem. B* **2005**, *109*, 13857–13870.

83. Sau, T. K.; Murphy, C. J. Self-Assembly Patterns Formed Upon Solvent Evaporation of Aqueous Cetyltrimethylammonium Bromide-Coated Gold Nanoparticles of Various Shapes. *Langmuir* **2005**, *21*, 2923–2929.

84. Pramod, B. P.; Thomas, K. G. Plasmon Coupling in Dimers of Au Nanorods. *Adv. Mater.* **2008**, *20*, 4300–4305.

85. Kou, X.; Zhang, S.; Yang, Z.; Tsung, C. K.; Stucky, G. D.; Sun, L.; Wang, J.; Yan, C. Glutathione- and Cysteine-Induced Transverse Overgrowth on Gold Nanorods. *J. Am. Chem. Soc.* **2007**, *129*, 6402–6404.

86. Maltzahn, G.; Park, J.; Agrawal, A.; Bandaru, N. K.; Das, S. K.; Sailor, M. J.; Bhatia, S. N. Computationally Guided Photothermal Tumor Therapy Using Long-Circulating Gold Nanorod Antennas. *Cancer Res.* **2009**, *69*, 3892–3901.

87. Porter, L.; Ji, D.; Westcott, S. L.; Graupe, M.; Czernuszewicz, R. S.; Halas, N. J.; Lee, T. R. Gold and Silver Nanoparticles Functionalized by the Adsorption of Dialkyl Disulfides. *Langmuir* **1998**, *14*, 7378–7386.

88. Gole, A.; Murphy, C. J. Polyelectrolyte-Coated Gold Nanorods : Synthesis , Characterization and Immobilization. *Chem. Mater.* **2005**, *17*, 1325–1330.

89. Ni, W. H.; Yang, Z.; Chen, H. J.; Li, L.; Wang, J. F. *J. Am. Chem. Soc.* **2008**, *130*, 6692.

90. Jaque, D.; Martinez Maestro, L.; Del Rosal, B.; Haro-Gonzalez, P.; Benayas, A.; Plaza, J. L.; Martin Rodriguez, E.; Garcia Sole, J. Nanoparticles for photothermal therapies. *Nanoscale* **2014**, *6*, 9494–9530.

91. Mackowiak, P. A. Principles and practice of infectious diseases. **2000**, *6*, 703–718.

92. Huff, T. B.; Zhao, Y.; Hansen, M. N.; Cheng, J.; Wei, A. Hyperthermic effects of gold nanorods on tumor cells. *Nanomedicine* **2007**, *2*, 125–132.

93. Huang, X.; El-Sayed, I. V.; Qian, W.; El-Sayed, M. A. Cancer Cell Imaging and Photothermal Therapy in the Near-Infrared Region by Using Gold Nanorods Cancer Cell Imaging and Photothermal Therapy in the Near-Infrared Region by Using Gold Nanorods. *J. Am. Chem. Soc.* **2006**, *128*, 2115-2120.

94. Hu, K. W.; Liu, T. M.; Chung, K. Y.; Huang, K. S.; Hsieh, C. T.; Sun, C. K.; Yeh, C. H. Efficient near-IR hyperthermia and intense nonlinear optical imaging contrast on the gold nanorod-in-shell nanostructures. *J. Am. Chem. Soc.* **2009**, *131*, 14186–14187.

95. Jang, B.; Park, J. Y.; Tung, C. H.; Kim, I. H.; Choi, Y. Gold Nanorod - Photosensitizer Complex for Near-Infrared Fluorescence Imaging and Photodynamic/ Photothermal Therapy In Vivo. *ACS Nano* **2011**, *5*, 1086–1094.

96. Aubry, J. M.; Pierlot, C.; Rigaudy, J.; Schmidt, R. Reversible Binding of Oxygen to Aromatic Compounds. *Acc. Chem. Res.* **2003**, *36*, 668–675.

97. Foote, C. S.; Wexler, S. Olefin oxidations with excited singlet oxygen. *J. Am. Chem. Soc.* **1964**, *86*, 3879–3880.

98. Rigaudy, J.; Dele´tang, C.; Basselier, J. J. Effet des substituants sur la photooxydation des syste`mes aromatiques. Premier exemple d'isolement d'un photooxyde en se´rie naphtale´nique; sa dissociation thermique. *Comptes Rendus Acad. Sci.* **1996**, *263(C)*, 1435–1438.

99. Saito, I.; Matsuura, T.; Inoue, K. Formation of Superoxide Ion from Singlet Oxygen. On the Use of a Water-Soluble Singlet Oxygen Source. *J. Am. Chem. Soc.* **1981**, *103*, 188–190.

100. Clennan, E. L.; Foote, C. S.: *In Organic Peroxides*; New York, **1992**.

101. Stevens, B.; Perez, S. R.; Ors, J. A. Photoperoxidation of Unsaturated Organic Molecules. *J. Am. Chem. Soc.* **1974**, 6846–6850.

102. Sime, M. A. I. Novel Molecules of the Phane-type with p-Benzoquinone and Oxahornobenzene Moieties. **2000**, *13*, 583–585.

103. Van der Heuvel, C. J. M.; Verhoeven, J. W.; de Boer, T. J. A frontier orbital description of the reaction of singlet oxygen with simple aromatic systems. *Recl. Trav. Chim. Pays-Bas* **1980**, *99*, 280–284.

104. Aubry, J. M.; Mandard-Cazin, B.; Rougee, M.; Bensasson, R. V. Kinetic Studies of Singlet Oxygen [4 + 2]- Cycloadditions with Cyclic 1,3-Dienes in 28 Solvents. *J. Am. Chem. Soc.* **1995**, *117*, 9159–9164.

105. Bobrowski, M.; Liwo, A.; Oldziej, S.; Jeziorek, D. CAS MCSCF / CAS MCQDPT2 Study of the Mechanism of Singlet Oxygen Addition to 1 , 3-Butadiene and Benzene. *J. Am. Chem. Soc.* **2000**, *112*, 8112–8119.

106. Schweitzer, C.; Schmidt, R. Physical Mechanisms of Generation and Deactivation of Singlet Oxygen. *Chem. Rev.* **2003**, *103*, 1685-1757 .

107. Turro, N. J.; Chow, M. F.; Rigaudyo, J. Mechanism of Thermolysis of Endoperoxides of Aromatic Compounds. Activation Parameters, Magnetic Field, and Magnetic Isotope Effectst. *J. Am. Chem. Soc.* **1981**, *103*, 7218–7224.

108. Chen, H.; Shao, L.; Li, Q.; Wang, J. Gold nanorods and their plasmonic properties. *Chem. Soc. Rev.* **2013**, *42*, 2679–2724.

APPENDIX

A.1 Controlled Singlet Oxygen Generation via Plasmonic Heating of Gold Nanorods

A.1.1. ^{1}H and $^{1}CH_3$ NMR Spectra

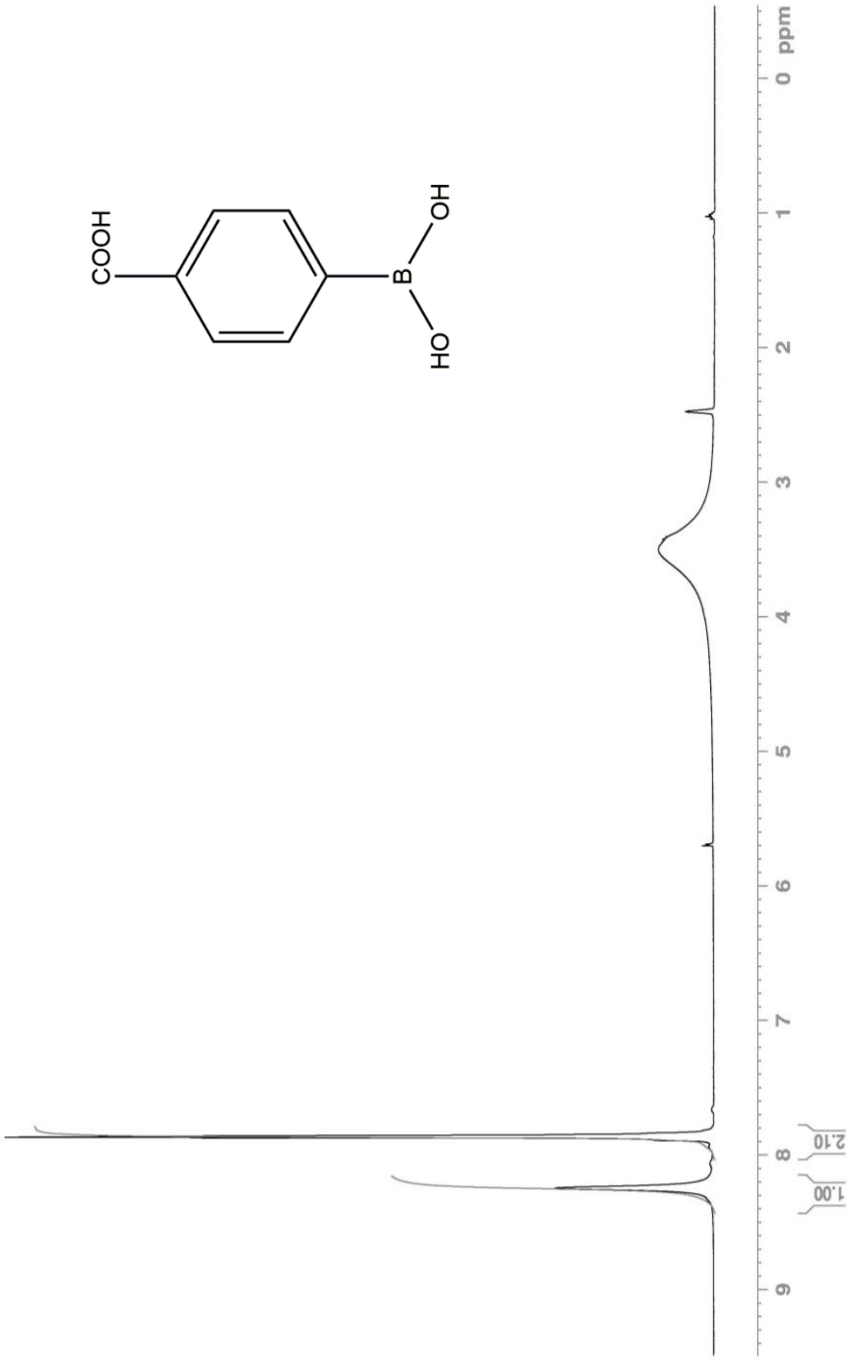

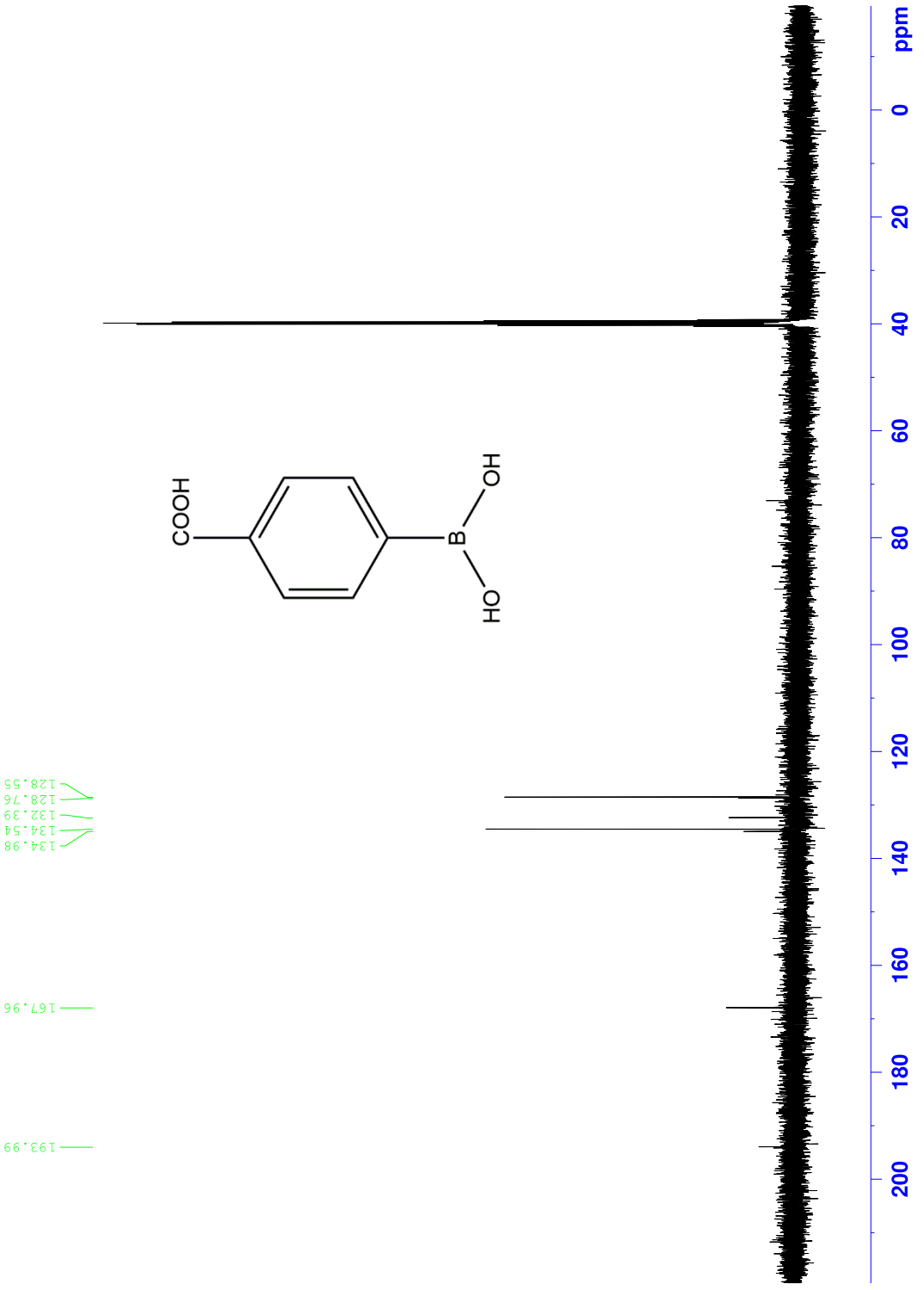
ppm
0
20
40
60
80
100
120
140
160
180
200
COOH
B
OH
HO
193.99
167.96
134.98
134.54
132.39
128.76
128.55

ppm
1
2
3
4
5
6
7
8
9
10
1.61
2.09
1.01
3279.739
3277.658
3126.490
3124.689
1502.085
1499.924
O
O
B
OH
HO

O
O
B
OH
HO
50.44
126.30
129.13
132.58
164.79
ppm

Br
3462.125
3453.282
3076.039
3067.237
3055.513
3054.672
3048.991
3047.790
3046.470
3039.067
3037.307
3035.586
3030.985
2978.528
2976.727
2970.485
2969.205
2962.683
2961.562
2960.522
2959.442
2953.920
2952.959
1.00
0.96
2.65
2.06
ppm

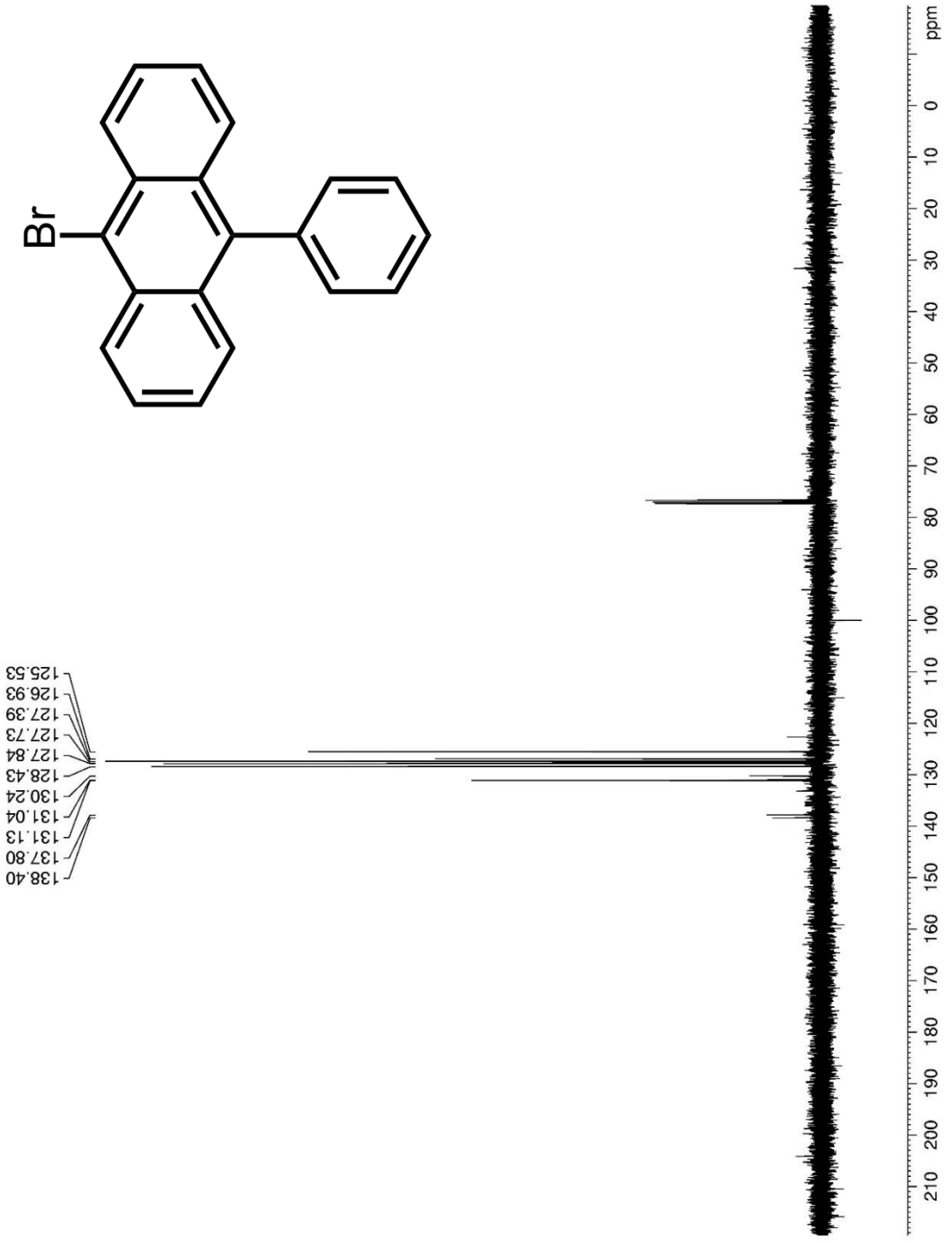
Br
138.40
137.80
131.13
131.04
130.24
128.43
127.84
127.73
127.39
126.93
125.53
ppm

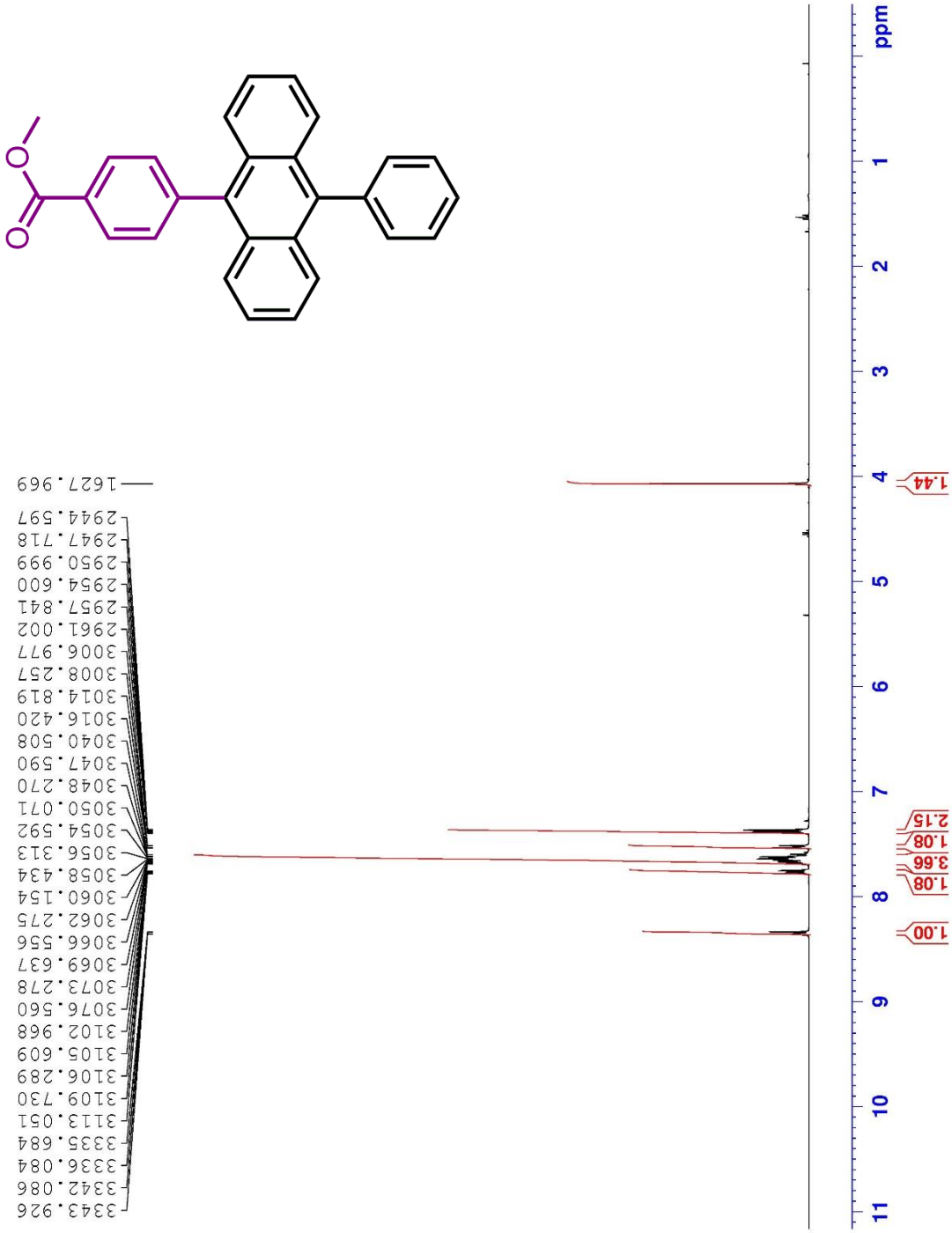
ppm
1
2
3
4
5
6
7
8
9
10
11
1.44
2.15
1.08
3.66
1.08
1.00
1627.969
2944.597
2947.718
2950.999
2954.600
2957.841
2961.002
3006.977
3008.257
3014.819
3016.420
3040.508
3047.590
3048.270
3050.071
3054.592
3056.313
3058.434
3060.154
3062.275
3066.556
3069.637
3073.278
3076.560
3102.968
3105.609
3106.289
3109.730
3113.051
3335.684
3336.084
3342.086
3343.926


14.48
52.26
61.14
125.14
125.39
125.40
126.50
126.52
127.14
127.60
128.48
129.51
129.58
129.73
129.77
129.88
131.29
131.53
131.58
135.77
137.76
138.93
144.37
167.10
ppm
0
10
20
30
40
50
60
70
80
90
100
110
120
130
140
150
160
170
180
190
200
210

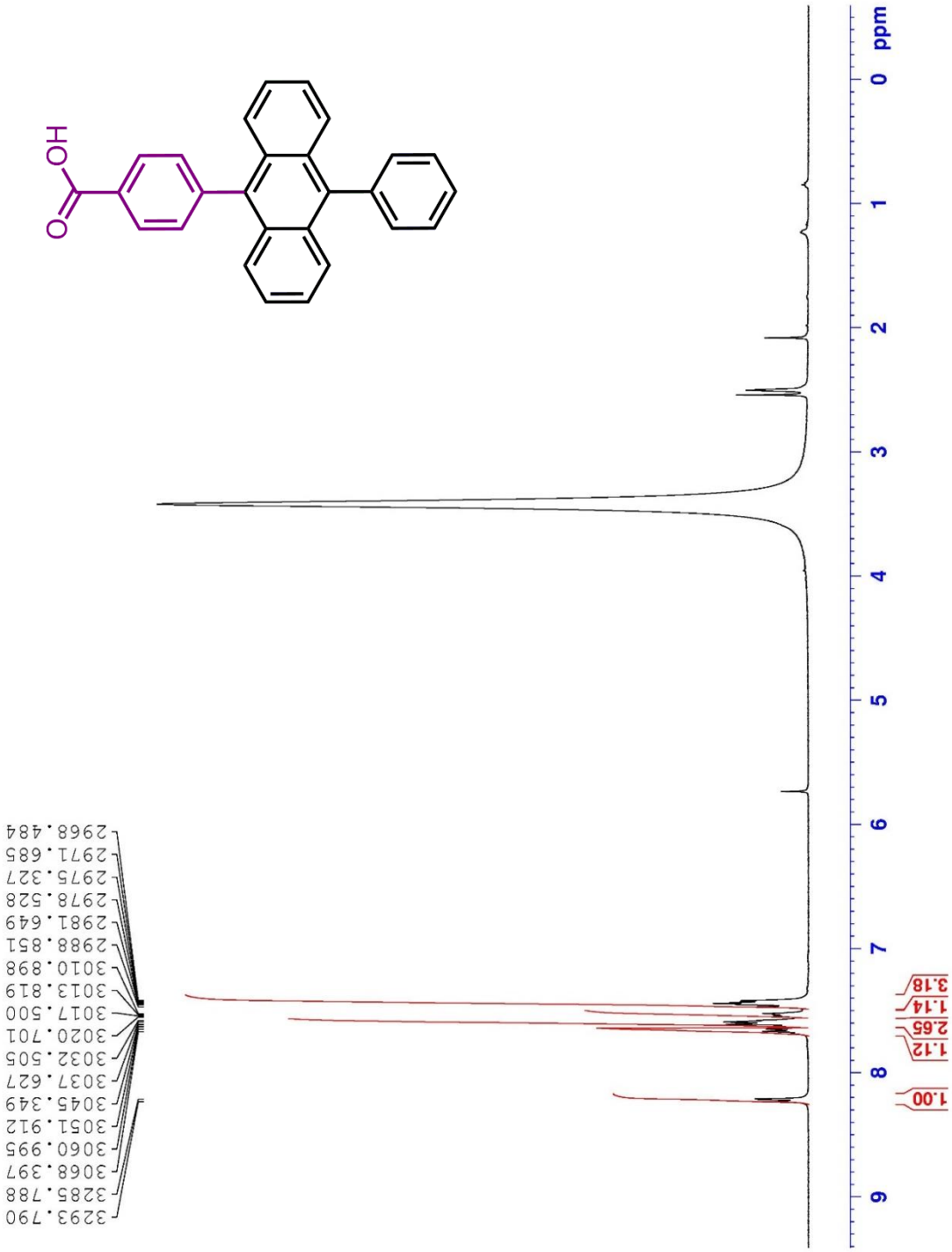
OH
O
ppm
0
1
2
3
4
5
6
7
8
9
3.18
1.14
2.65
1.12
1.00
2968.484
2971.685
2975.327
2978.528
2981.649
2988.851
3010.898
3013.819
3017.500
3020.701
3032.505
3037.627
3045.349
3051.912
3060.995
3068.397
3285.788
3293.790

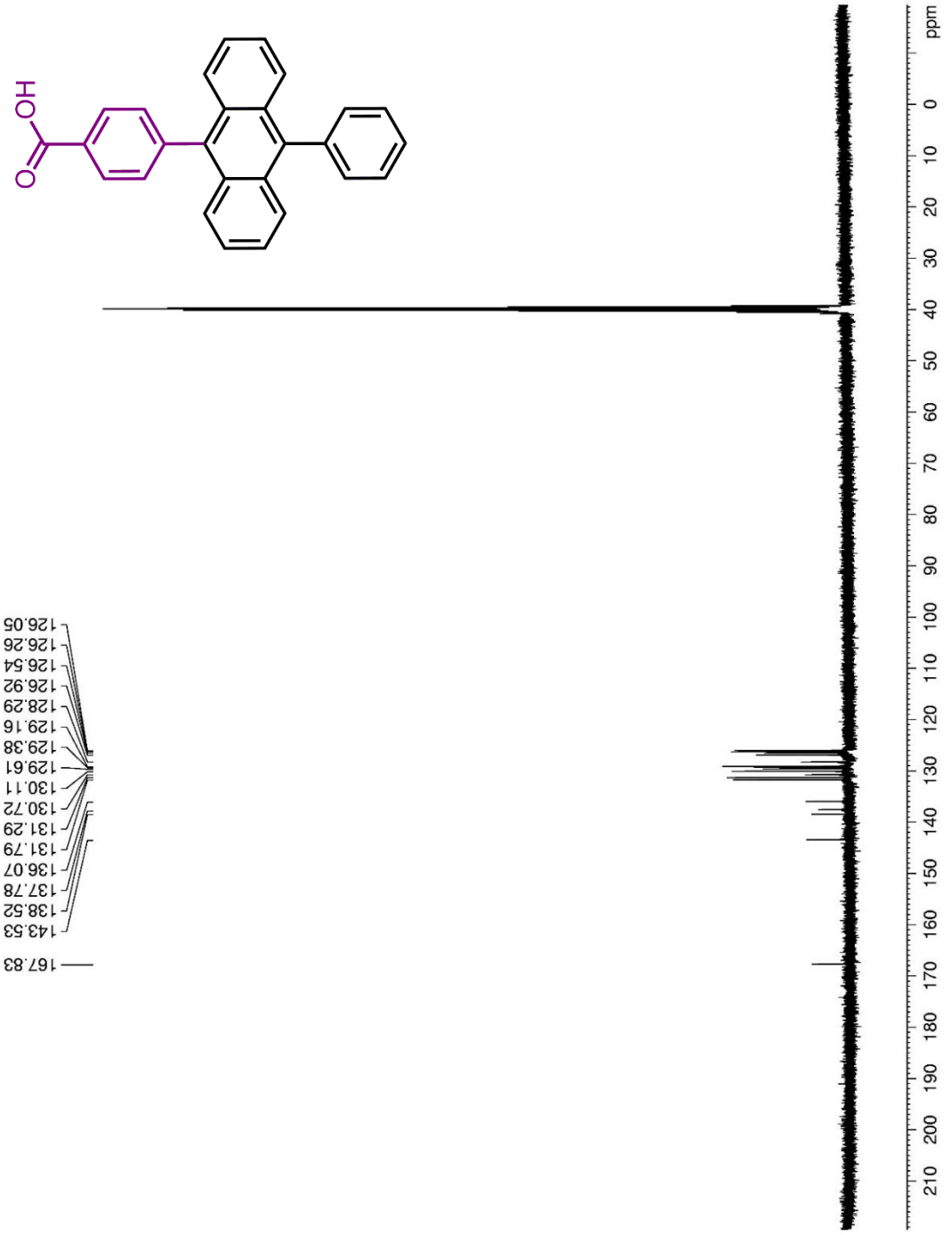
HO
O
167.83
143.53
138.52
137.78
136.07
131.79
131.29
130.72
130.11
129.61
129.38
129.16
128.29
126.92
126.54
126.26
126.05
ppm
0
10
20
30
40
50
60
70
80
90
100
110
120
130
140
150
160
170
180
190
200
210

OH
O
O
O
ppm
1
2
3
4
5
6
7
8
9
10
2.10
2.09
1.60
1.05
0.94
1.00
3311.396
3309.915
3303.233
3301.553
3116.573
3115.052
3108.290
3088.043
3081.121
3063.555
3061.675
3055.353
3053.432
2935.314
2932.633
2930.192
2928.752
2927.871
2922.630
2845.484
2843.204
2841.483
2839.042
2836.802
2833.801
2831.960
2829.439
2827.599
2824.998

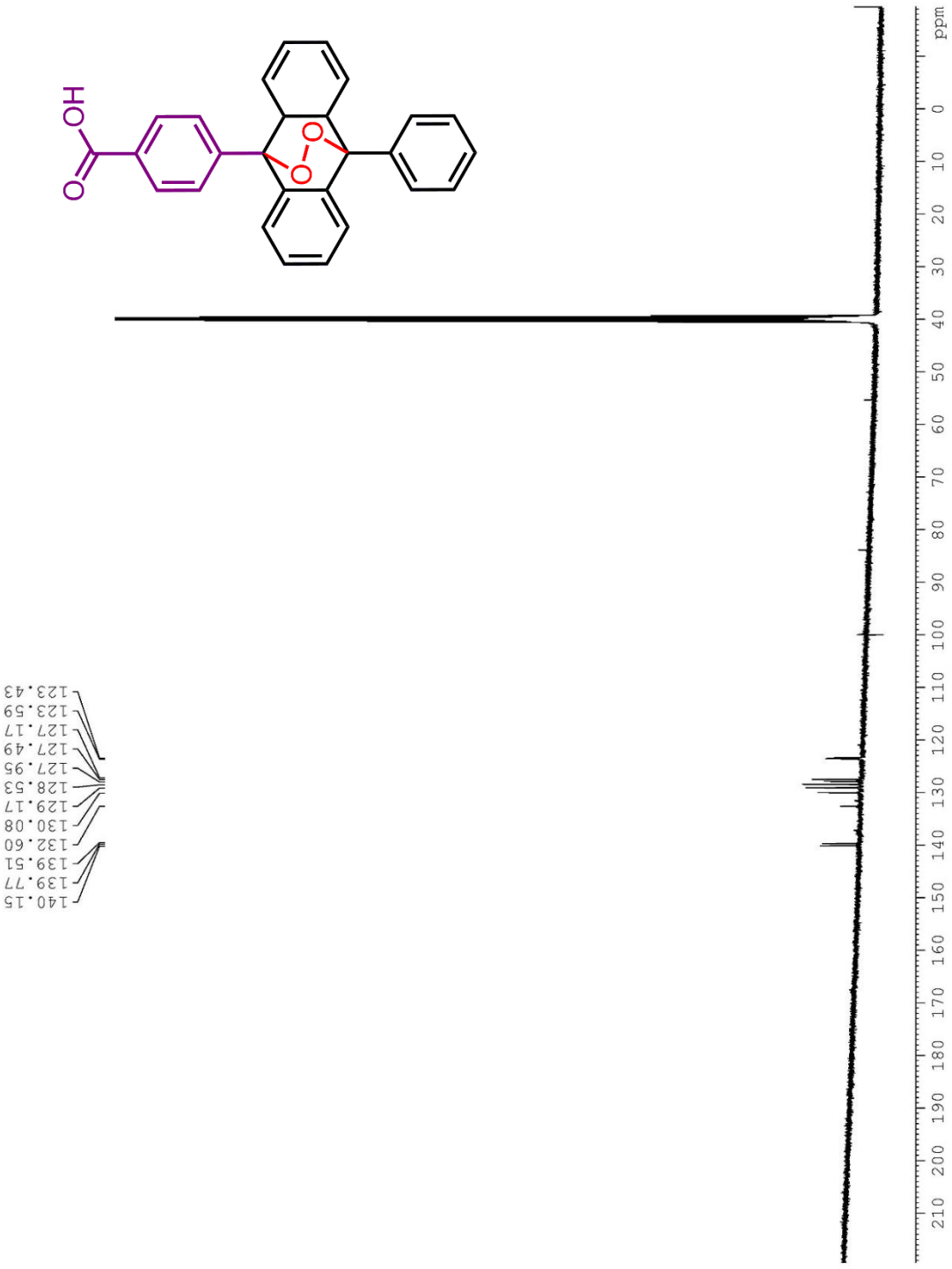
HO
O
O
O
ppm
0
10
20
30
40
50
60
70
80
90
100
110
120
130
140
150
160
170
180
190
200
210
140.15
139.77
139.51
132.60
130.08
129.17
128.53
127.95
127.49
127.17
123.59
123.43

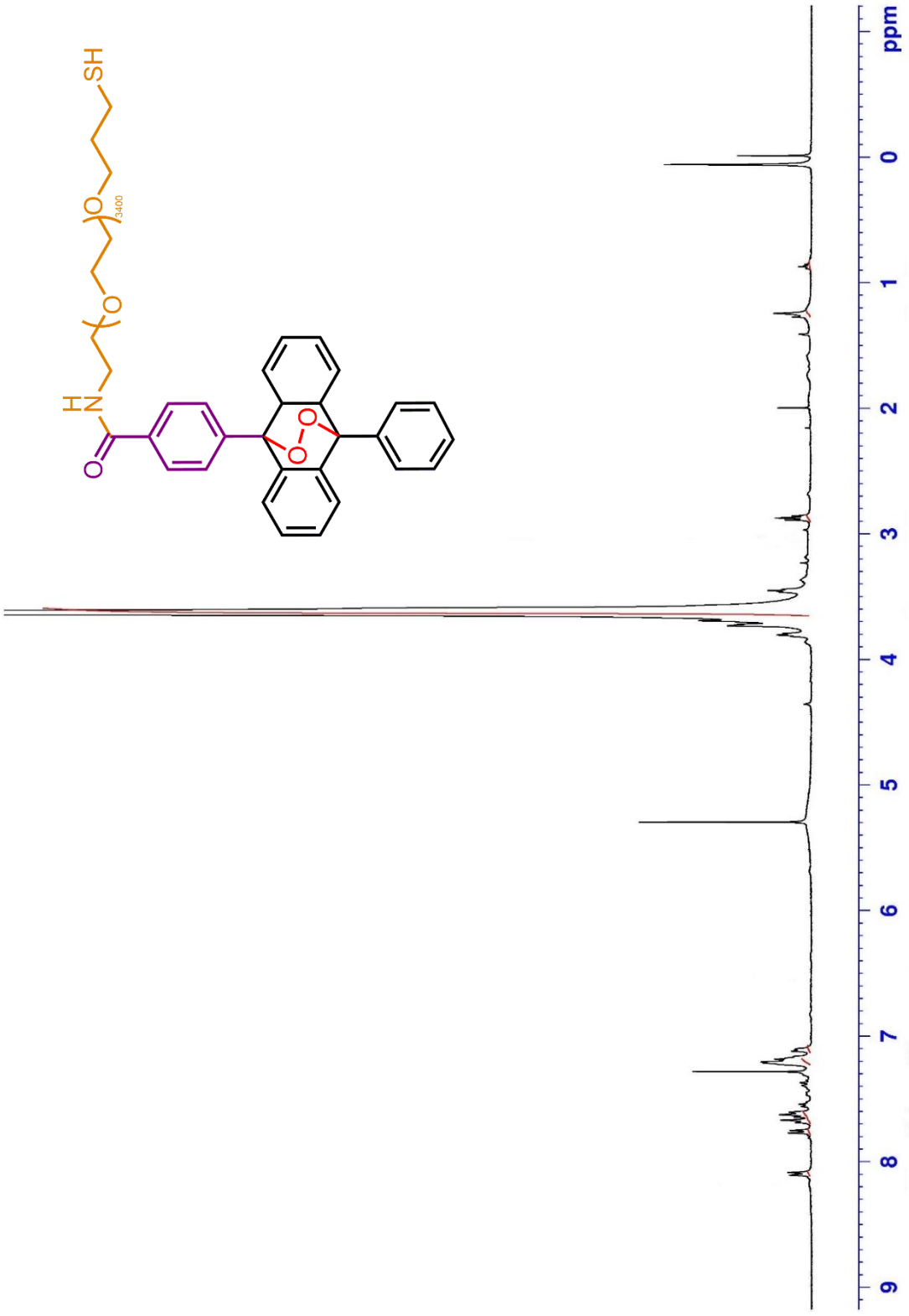
SH
O
3400
O
H
N
O
O
O
ppm
0
1
2
3
4
5
6
7
8
9

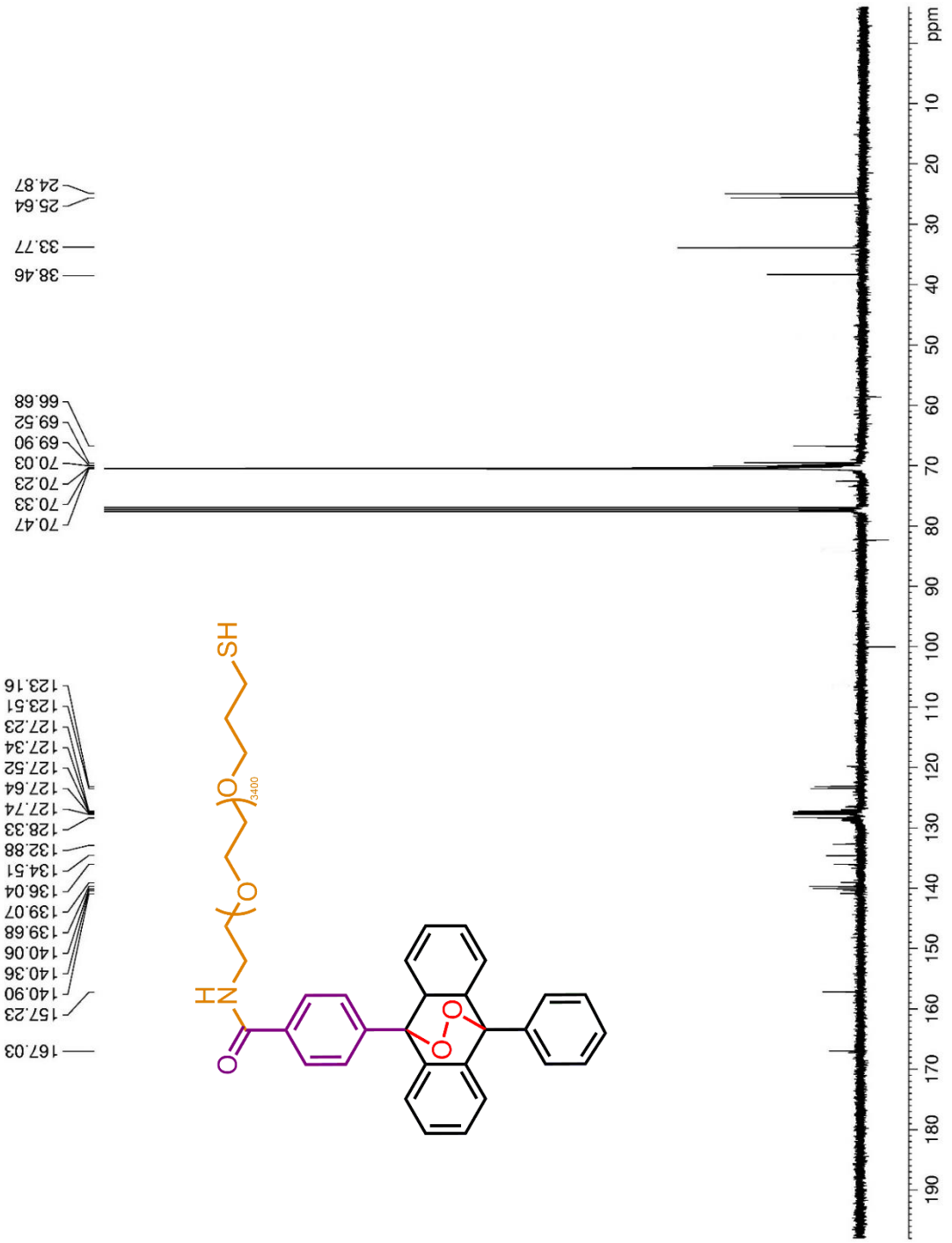
24.87
25.64
33.77
38.46
66.68
69.52
69.90
70.03
70.23
70.33
70.47
123.16
123.51
127.23
127.34
127.52
127.64
127.74
128.33
132.88
134.51
136.04
139.07
139.68
140.06
140.36
140.90
157.23
167.03
SH
O
3400
O
O
N
H
O
O
ppm
10
20
30
40
50
60
70
80
90
100
110
120
130
140
150
160
170
180
190

A.1.2. Mass Spectra

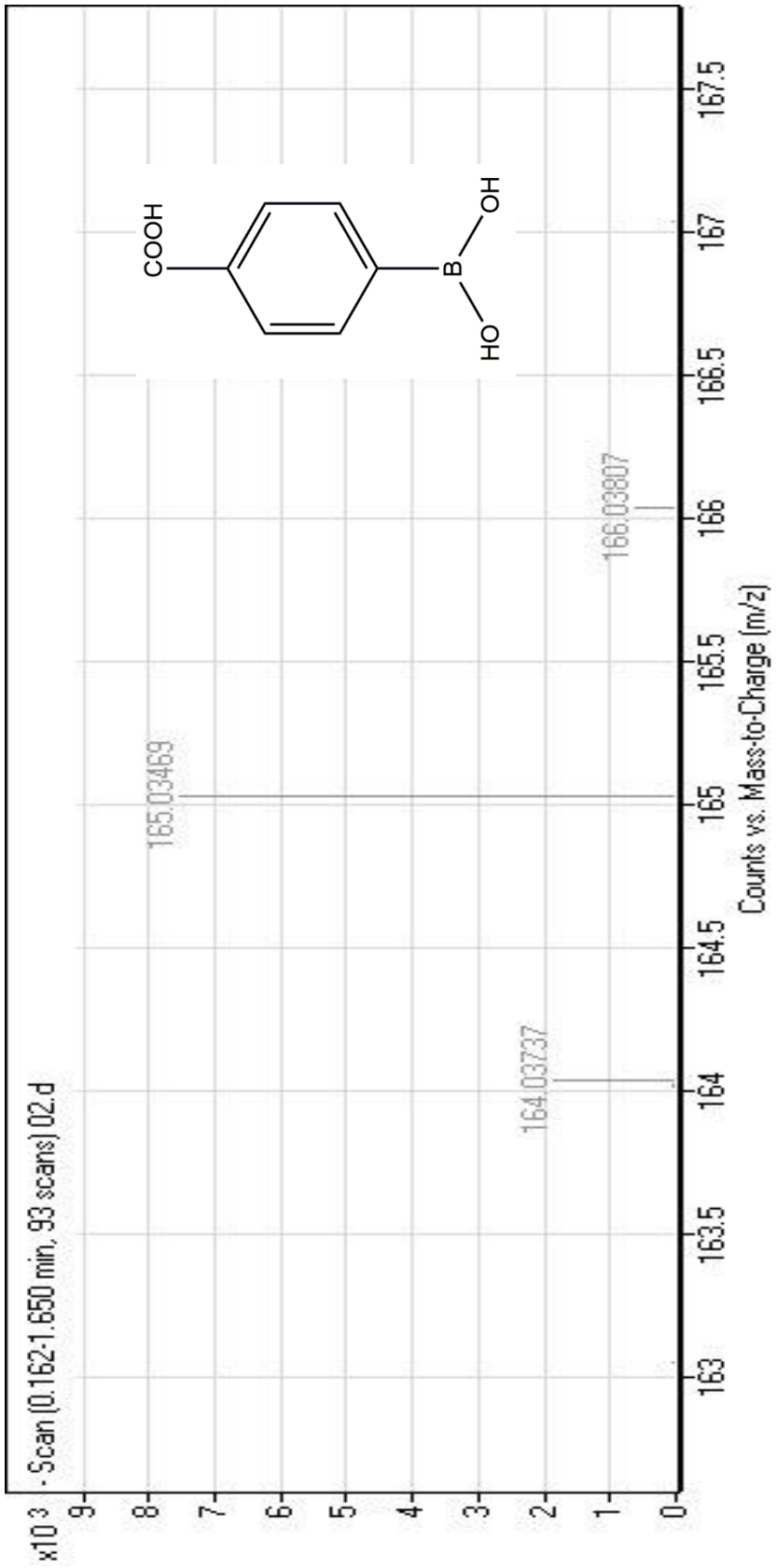

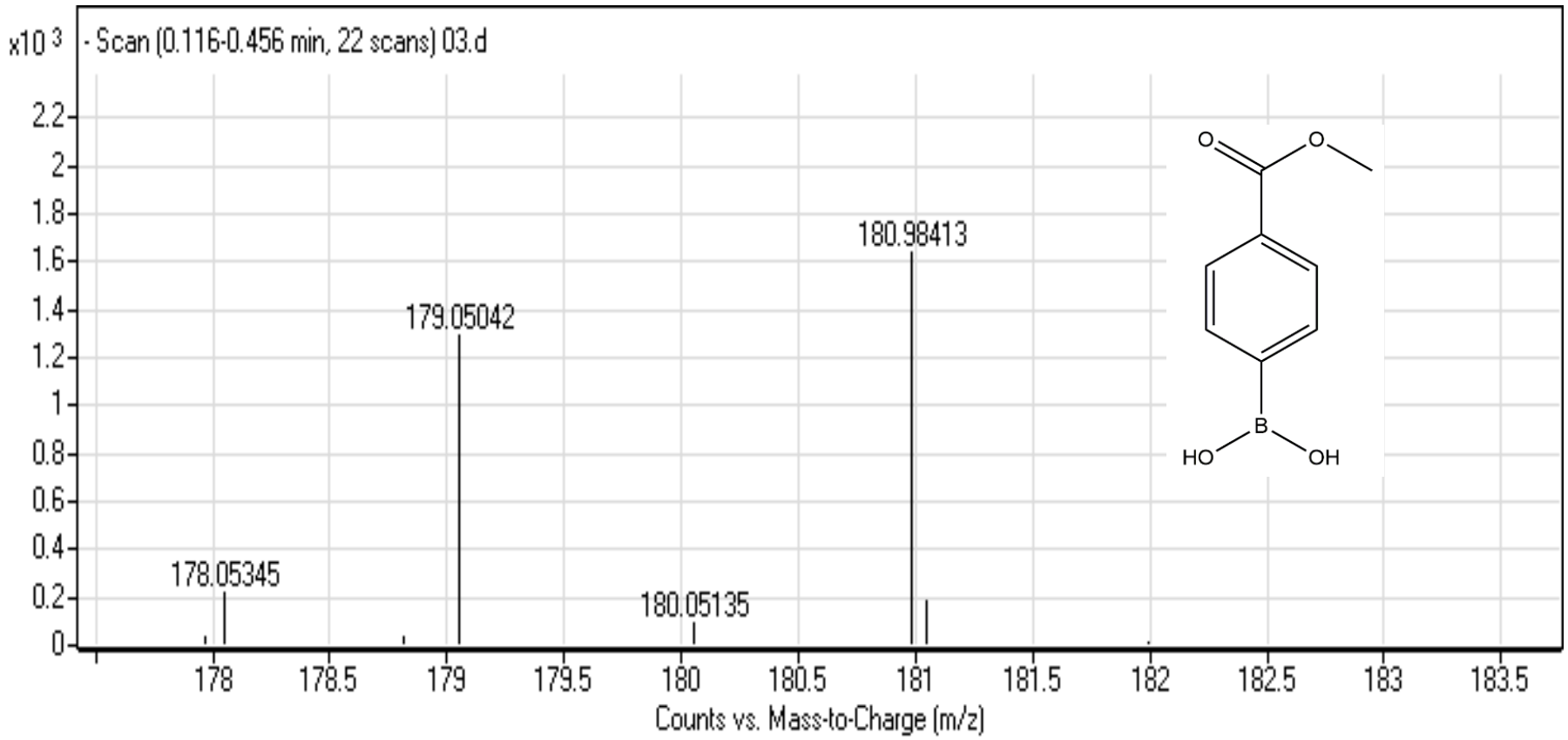
x10 3
- Scan (0.116-0.456 min, 22 scans) 03.d
2.2
2
1.8
1.6
1.4
1.2
1
0.8
0.6
0.4
0.2
0
178.05345
179.05042
180.05135
180.98413
178
178.5
179
179.5
180
180.5
181
181.5
182
182.5
183
183.5
Counts vs. Mass-to-Charge (m/z)
O
O
B
HO
OH

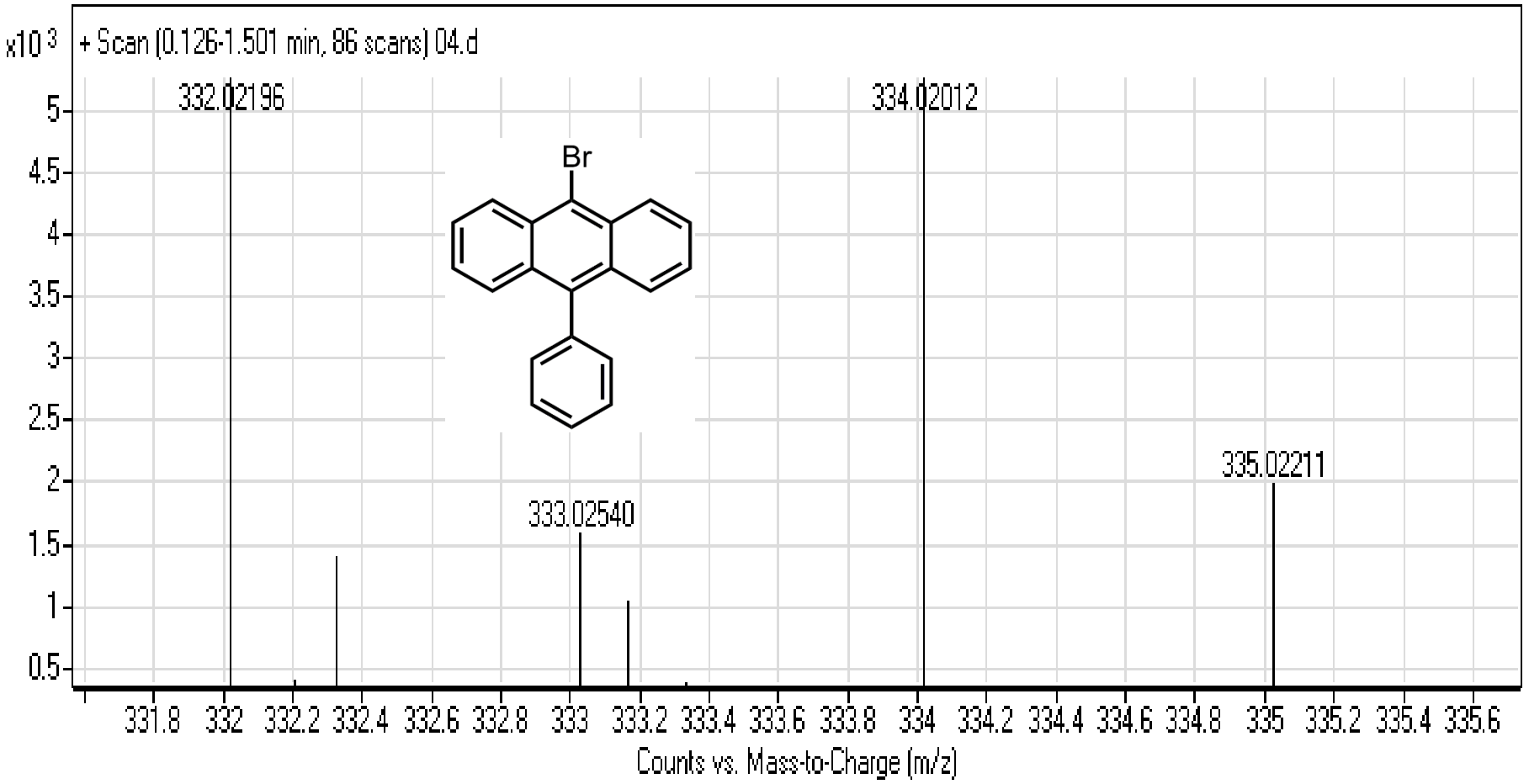
+ Scan (0.126-1.501 min, 86 scans) 04.d
x10 3
5
4.5
4
3.5
3
2.5
2
1.5
1
0.5
332.02196
334.02012
335.02211
333.02540
Br
331.8 332 332.2 332.4 332.6 332.8 333 333.2 333.4 333.6 333.8 334 334.2 334.4 334.6 334.8 335 335.2 335.4 335.6
Counts vs. Mass-to-Charge (m/z)

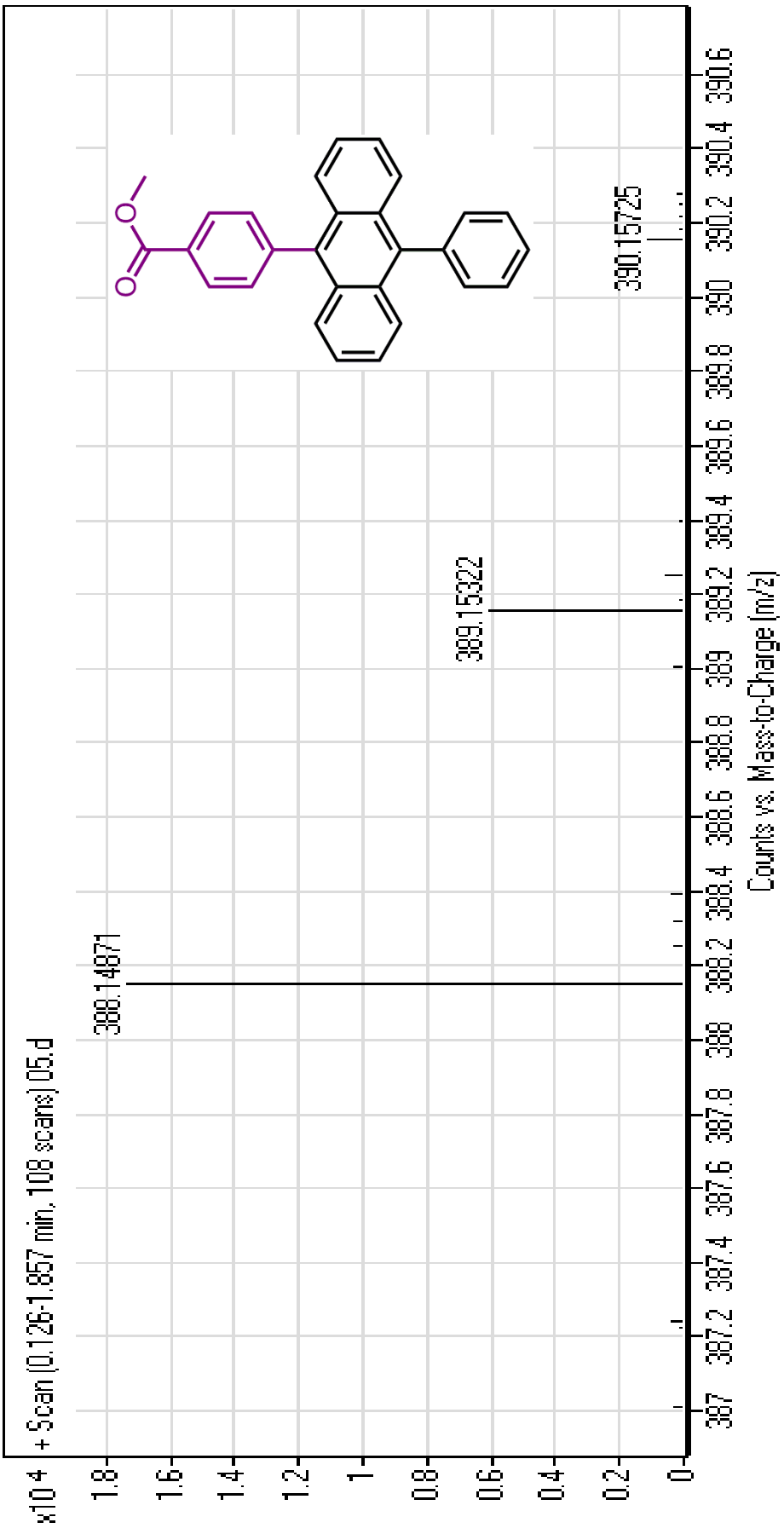
x10 4
+ Scan (0.126-1.857 min, 108 scans) 05.d
388.14871
389.15322
390.15725
Counts vs. Mass-to-Charge (m/z)

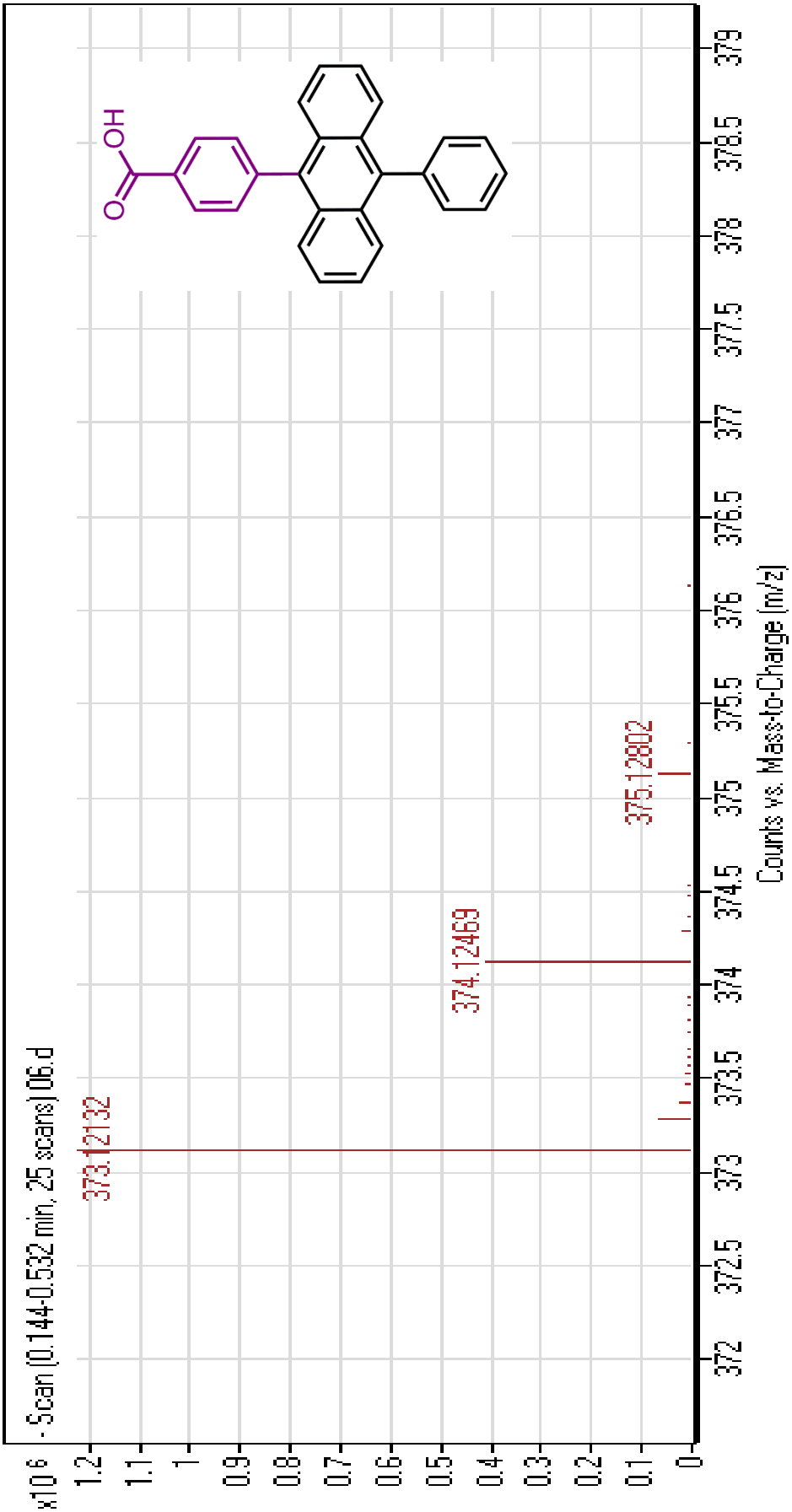
- Scan (0.144-0.532 min, 25 scans) 06.d
x10 6
1.2
1.1
1
0.9
0.8
0.7
0.6
0.5
0.4
0.3
0.2
0.1
0
373.12132
374.12469
375.12802
372
372.5
373
373.5
374
374.5
375
375.5
376
376.5
377
377.5
378
378.5
379
Counts vs. Mass-to-Charge (m/z)
OH
O

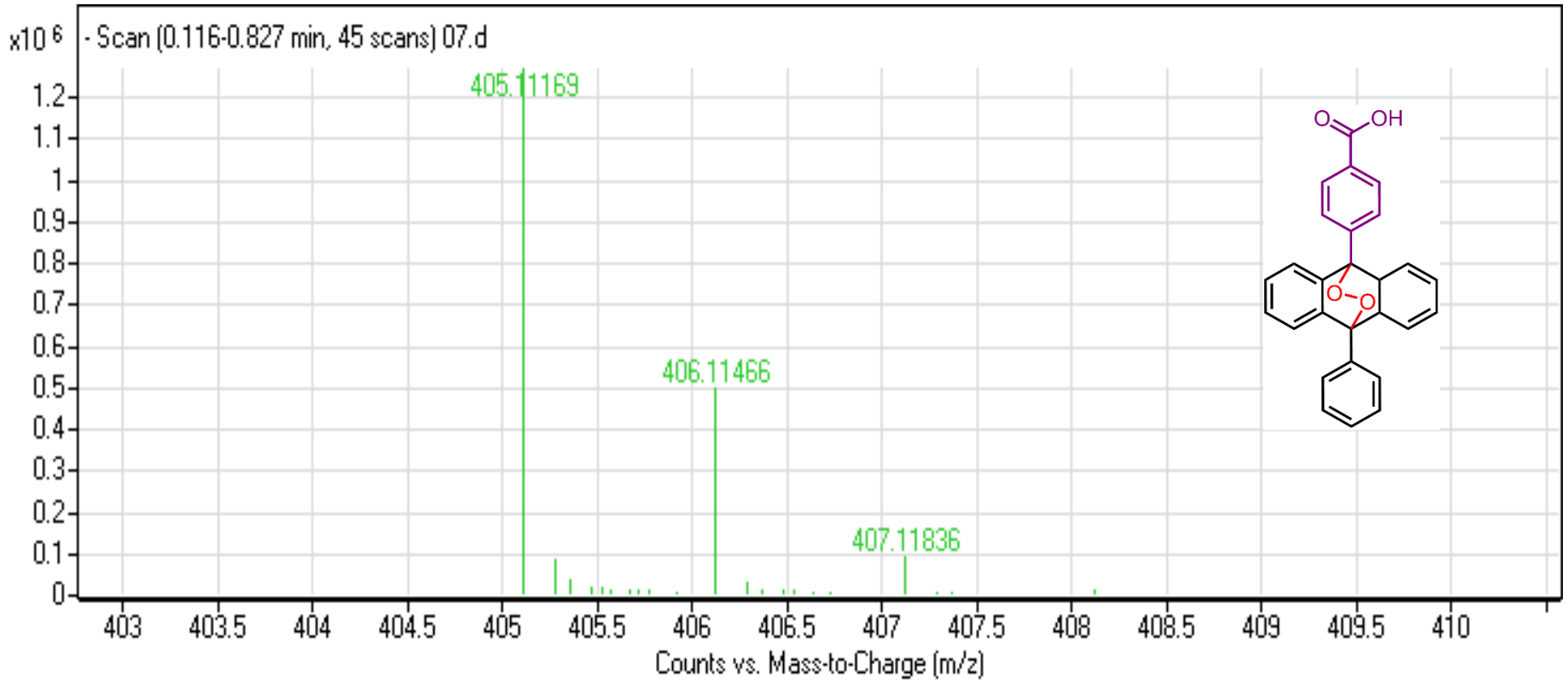
x10 6
- Scan (0.116-0.827 min, 45 scans) 07.d
405.11169
406.11466
407.11836
1.2
1.1
1
0.9
0.8
0.7
0.6
0.5
0.4
0.3
0.2
0.1
0
403
403.5
404
404.5
405
405.5
406
406.5
407
407.5
408
408.5
409
409.5
410
Counts vs. Mass-to-Charge (m/z)
O
OH
O
O